Solid State Spectroscopy I
— IR, VUV, etc. —

(BL1B, 3A1, 6A1, 7A, 7B)

(BL1B)

Vacuum-ultraviolet reflectance spectroscopy of transition-metal oxides

Yoshinori TOKURA [1,2,3], Shigeki MIYASAKA [2], Yasujiro TAGUCHI [1], Katsuhiro TOBE [1], Kyoko ISHIZAKA [1], Takahumi SAITO [4], and Taka-hisa ARIMA [4]

[1] *Department of Applied Physics, University of Tokyo, Tokyo 113-8656*

[2] *Joint Research Center for Atom Technology (JRCAT), Tsukuba 305-0046*

[3] *Correlated Electron Reseach Center (CERC), National Institute of Advanced Industrial Science and Technology(AIST), Tsukuba 305-0046*

[4] *Institute of Materials Science, University of Tukuba, Tsukuba 305-8573*

One of the most important characteristics of the correlated electron systems is the drastic re-construction of electronic structure over an energy scale of eV with changes of temperature, doping concentration, and/or external field. Therefore, optical reflectivity measurement over a wide energy range and the optical conductivity spectra derived from the reflectivity spectra provide us with very useful information about the strongly correlated electron systems.

We measured the reflectivity spectra of several transition-metal oxides, including Mn-, Ni-, Co-, Mo- and V-oxides, for an energy range of 4 eV < E < 35 eV at room temperature using the beam line BL1B. The measured reflectivity data, together with the lower-energy data below 6 eV, were used to derive the optical conductivity spectra or dielectric function via the Kramers-Kronig analysis. As an example, imaginary part of the dielectric function of perovskite-type V-oxide, YVO_3, are shown below.

This compound is well known as a typical Mott-Hubbard insulator that has orbital-ordered ground state as well as intermediate-temperature phase whose patterns determine the respective spin-ordering pattern (G-type and C-type). The compound is also of current great interest because of thermally induced magnetization reversal. As shown in the figure, the ε_2 spectra show small anisotropy even at room temperature, which is above the spin- and orbital-ordering temperatures. These spectral features are attributed to robust spin- and orbital-correlation .

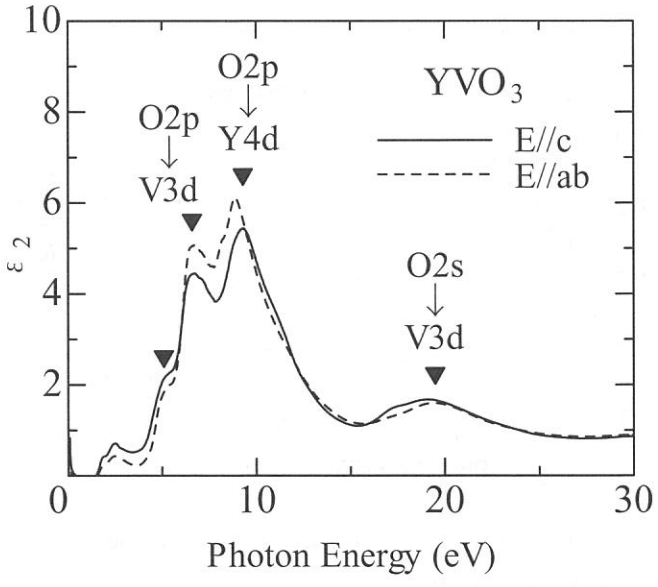

(BL1B)

Extreme-Ultraviolet Reflectivity Spectra and Electronic Structures of $PbWO_4$

Masami FUJITA

Japan Coast Guard Academy, Wakaba, Kure 737-8512

Hiroshi YOKOTA, Yoshiyuki INABE, Michihiro HORIMOTO and Minoru ITOH

Department of Electrical and Electronic Engineering, Shinshu University, Nagano 380-8553

Lead tungstate ($PbWO_4$) has been received intense attention as a promising candidate for scintillating substance [1]. On the other hand, its basic optical properties, such as reflectivity spectra or dielectric constants, have not been established experimentally until now. Very recently, remarkable dichroism has been observed on the reflectivity spectra by us [2] and other groups [3,4]. However, there are some discrepancies among these results. In the present study, polarized reflectivity spectra of $PbWO_4$ crystals with scheelite structure have been measured in the extreme ultraviolet up to 30 eV.

Single crystals of $PbWO_4$ were obtained from the Institute of Solid State Physics of Russian Academy of Sciences and the Materials Research Laboratory of Furukawa Company. Reflectivity spectra were measured at 8 K on the cleaved surfaces of (011) plane, with the electric vector parallel ($\boldsymbol{E} \parallel \boldsymbol{a}$) and perpendicular ($\boldsymbol{E} \perp \boldsymbol{a}$) to the a-axis [2].

Figure 1 shows typical reflectivity spectra of $PbWO_4$ in the 3–30 eV region. A strong exciton band 1 is observed for the polarization $\boldsymbol{E} \parallel \boldsymbol{a}$. The intensity of the exciton band 1 for $\boldsymbol{E} \perp \boldsymbol{a}$ is very small. Several polarization-dependent structures are also observed in the high-energy region. A strong peak 2 is observed at 5.3 eV for $\boldsymbol{E} \perp \boldsymbol{a}$, while such a peak is not observed for $\boldsymbol{E} \parallel \boldsymbol{a}$. One may see a structure 3 around 6.5 eV. The broad peak 4 observed for both polarizations probably corresponds to the prominent peak observed in the 8–9 eV region in Refs. 3 and 4. The reflectivity decreases gradually above 9 eV and shows a minimum at around 12–14 eV. The structures in the 4–10 eV region are mainly ascribed to the transitions from the valence band to

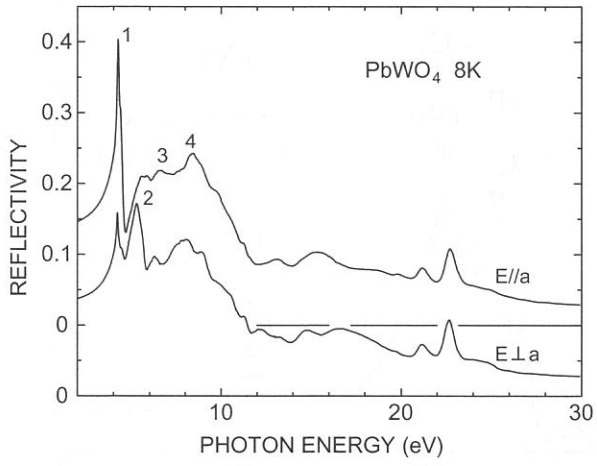

Fig. 1 Reflectivity spectra of scheelite $PbWO_4$ in the 3–30 eV region at 8 K.

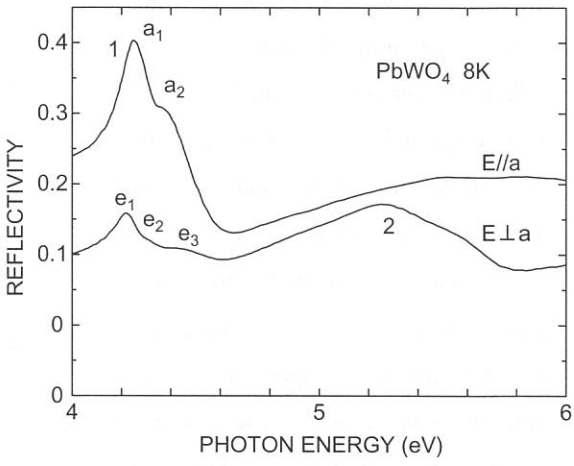

Fig. 2 Reflectivity spectra of scheelite $PbWO_4$ in the exciton-band region at 8 K.

the bottom of the conduction band, since the calculated width of the valence band is about 5.5 eV (see below). Sharp peaks due to the transition from the Pb^{2+} 5*d* core level to the 6*p* level are observed in the 19–25 eV region, indicating that the Pb^{2+} 6*p* state contributes appreciably to the bottom of the conduction band. It is supposed that the exciton transition in $PbWO_4$ would involve the cationic Pb^{2+} $6s \rightarrow 6p$ excitation as well as the charge transfer from oxygen to tungsten.

In Fig. 2 are shown reflectivity spectra in the exciton-band region on an expanded scale. We can see two structures a_1 and a_2 for the polarization $\boldsymbol{E} \,//\, \boldsymbol{a}$ and three structures e_1, e_2 and e_3 for $\boldsymbol{E} \perp \boldsymbol{a}$. The fine structures a_1 (e_1) and a_2 (e_2) would originate from the spin-orbit splitting of the Pb^{2+} 6*p* state. The structure e_3 is likely to be assigned to the longitudinal exciton-polariton mode peculiar to anisotropic crystals, since the light wave with the polarization $\boldsymbol{E} \perp \boldsymbol{a}$ propagates as an extraordinary ray in the crystal.

We are now calculating the electronic structure of scheelite $PbWO_4$ by using the DV-Xα method. A preliminary result of simple $[PbW_4O_{16}]^{6-}$ cluster is presented in Fig. 3. It appears that the valence band is built up of mixed Pb(6*s*)-O(2*p*) state, and the conduction band is composed of mixed Pb(6*p*)-W(5*d*) state. This result is fairly consistent with the above interpretation of the fine structures in the exciton-band region.

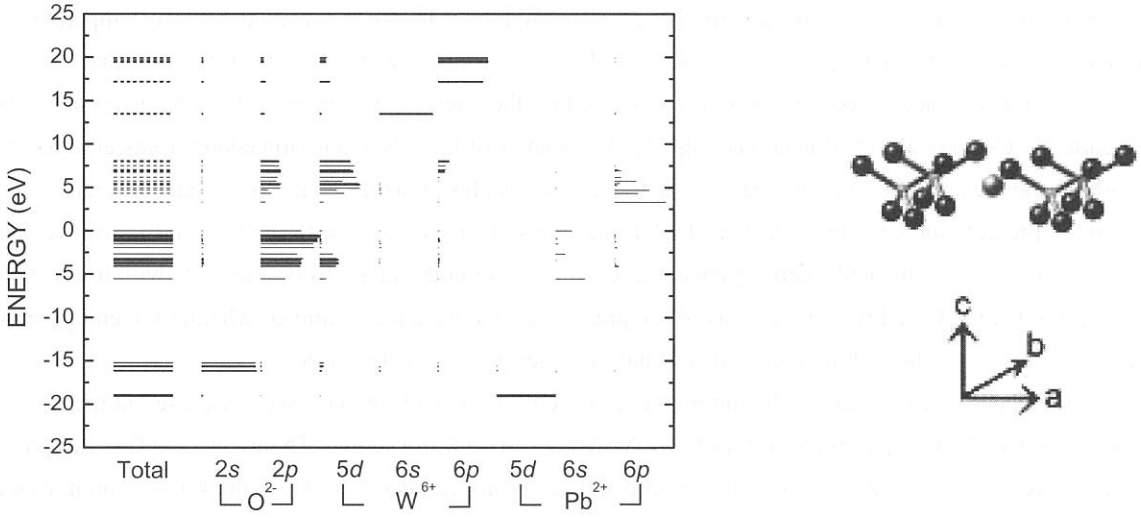

Fig. 3 Electronic structure of $PbWO_4$ calculated by DV-Xα method (right-hand side: simple $[PbW_4O_{16}]^{6-}$ cluster).

The authors would like to thank Dr. D. L. Alov and Dr. Y. Usuki for supplying the single crystals.

References

[1] M. Nikl: Phys. Status Solidi A **178** (2000) 595.

[2] M. Fujita, M. Itoh, M. Horimoto, Y. Usuki, M. Kobayashi and M. Nikl: J. Phys. Soc. Jpn. **70** (2001) 1439.

[3] I. A. Kamenskikh, V. N. Kolobanov, V. V. Mikhailin, I. N. Shpinkov, D. A. Spassky and G. Zimmerer: Nucl. Instrum. Methods Phys. Res. A **467-468** (2001) 1423.

[4] M. Kirm *et al.*: *Proc. 9th Int. Symposium on the Physics and Chemistry of Luminescent Materials*, ed. C. Ronda and A. M. Srivastava (Electrochemical Society, Pennington, NJ) in press.

(BL1B)

Luminescence of CuI Microcrystals Dispersed in KI Matrix under Matrix Excitation

[A]T. HIRAI, [B]Y. HARADA, [C]S. HASHIMOTO and [A]T. ITOH

[A]*Division of Materials Physics, Graduate School of Engineering Science, Osaka University, Toyonaka, 560-8531, Japan*

[B]*Applied Physics, Osaka Institute of Technology, Osaka, 535-8585, Japan*

[C]*Department of Environmental Science, Faculty of Science, Osaka Women's University, Sakai, 590-0035, Japan*

Lots of studies have been conducted on optical properties of semiconductor mesoscopic particles dispersed in insulator matrices so far. Almost all the studies have focused on the optical properties of the semiconductor particles in the visible or near ultraviolet spectral regions. Accordingly, we have focused our attention on the far and vacuum ultraviolet spectroscopy of the semiconductor particles dispersed in insulator matrices.

One of our great interests in this subject is the excitation energy transfer from the insulator matrix to the semiconductor particles through the interface. In other words, we expect that the excitation of the matrix by photons or electrons can efficiently give the luminescence of the semiconductor particles: the matrix-sensitized luminescence. In the past, KI crystals doped with Tl^+ impurity ions have been reported to occur the energy transfer to the Tl^+ impurity ions due to the exciton migration in the KI crystal at low temperature [1]. Furthermore, it has been recently proposed in CsI crystals doped with Na^+ impurity ions that the X-ray stimulated luminescence at room temperature is caused by the energy transfer carried by the electrons or holes created in the CsI crystal to NaI nano-crystals [2]. As a matter of fact, the excitation energy transfer is of utmost importance on the application to luminescent materials such as phosphors, laser and scintillator crystals.

In the present study, we have dealt with CuI microcrystals dispersed in a KI matrix, and have investigated the luminescence from the CuI microcrystals at low temperature in the range from 3 to 7 eV with use of SOR at BL1B in the UVSOR facility. On the basis of the present results, we have examined whether the energy transfer from the KI matrix to the CuI microcrystals through the interface is possible or not.

On the upper side of figure 1, the luminescence spectra of the CuI microcrystals dispersed in the KI crystal excited by (a) 4.13-eV, (b) 4.96-eV and (c) 6.42-eV photons at 10 K are shown. There exist the first exciton band of CuI and KI at 3.05 eV ($Z_{1,2}$ exciton) and 5.83 eV (1s exciton), respectively. Thus, the 4.13-eV photons excite only the CuI microcrystals, and most of the 6.42-eV photons are absorbed by the KI matrix. In addition, the absorption band around 4.7 eV and the luminescence band around 3.1 eV, which originate from isolated Cu^+ ions, can be observed in KI crystals doped with Cu^+ impurity ions [3]. Supposed that there are a lot of Cu^+ ions in the KI crystal, the 4.96-eV photons are expected to excite the Cu^+ ions. Firstly, we can see in Fig. 1(a) the luminescence line at 3.05 eV ascribed to bound excitons and the luminescence band around 2.95 eV due to donor-acceptor pair transitions, which come from CuI microcrystals regarded as bulk crystals. In addition, the luminescence at the higher-energy side of the luminescence line at 3.05 eV is probably assigned to confined excitons in CuI nano-crystals. Secondly in Fig. 1(b), the luminescence line and bands from the CuI microcrystals can be seen like Fig. 1(a). It should be pointed out that the luminescence band originating from the Cu^+ impurity ions is not observable. This fact suggests that very few Cu^+ ions are left in the KI crystal because they have almost precipitated as CuI microcrystals in our sample. Thirdly, there appear two luminescence bands ascribe to type I and type II self-trapped excitons (STEs) in KI at 4.15 eV and 3.31 eV in Fig. 1(c), compared to Fig.1 (a) and (b). From the results, we should notice that the luminescence of the CuI microcrystals around 3 eV could be observed in addition to the STE luminescence of KI even under the interband excitation of KI. Finally, Fig 1(d)

shows the excitation spectrum monitored at 3.05 eV at 10 K. Below ~ 5.5 eV, the spectrum corresponds to the optical transition of CuI. On the other hand, the spectrum above 6 eV is quite similar to the excitation spectrum for the luminescence band of Tl^+ ions reported in KI crystal heavily doped with Tl^+ ions [1], although the 3.05-eV luminescence contains not only the exciton luminescence of CuI but also the STE luminescence of KI. According to [1], the Tl^+ luminescence is caused by the energy transfer due to the exciton migration in the KI crystal. Consequently, the results suggest that the CuI luminescence under the excitation on the intrinsic absorption of KI is strongly correlated to the excitonic process in the KI matrix.

References

[1] H. Nishimura and M. Tomura, J. Phys. Soc. Japan, **39**, 390 (1975)
[2] H. Nishimura, Kotaibutsuri (in Japanese), **35**, 243 (2000)
[3] R. Oggioni and P. Scaramamelli, phys. stat. sol. , **9**, 411 (1965)

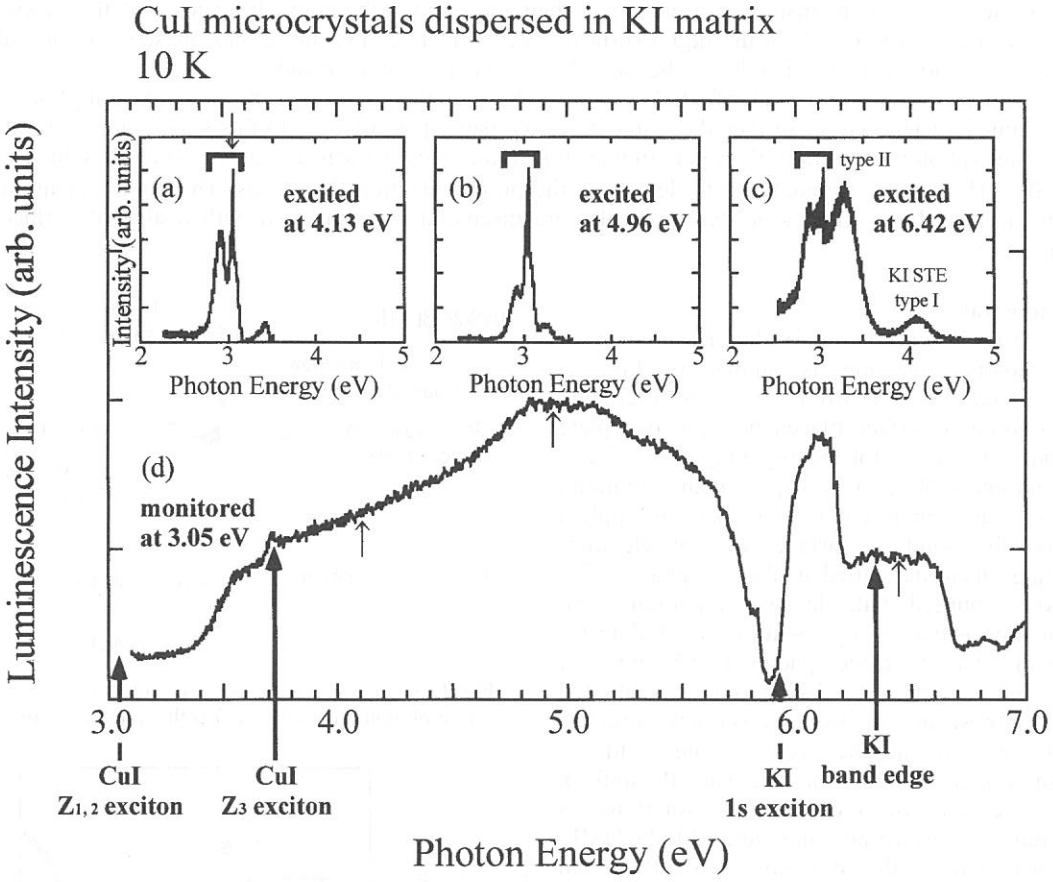

Figure 1. Luminescence spectra of CuI microcrystals dispersed in KI matrix excited at three different photon energies (upper) and the excitation spectrum monitored at 3.05 eV (lower) at 10 K.

(BL1B)

Photoionization of Adsorbed Rhodamine Dyes at the Aqueous Solution Surfaces

Toshio Ishioka, Koichiro Seno, Akira Harata, and Yoshihiko Hatano

Department of Molecular and Material Sciences, Interdisciplinary Graduate School of Engineering Sciences, Kyushu University, Kasugakoen 6-1, Kasuga-shi, Fukuoka 816-8680, Japan

Photoionization of molecules has been of great importance both in fundamental and applied sciences. Such studies have been in progress with powerful photon sources such as lasers and synchrotron radiation (SR).[1] SR covers higher and wider photon energy regions than laser radiation so that SR is used for the photoionizing of molecules not only in the gas phase but also in the condensed phase or at the surface to characterize molecular states or to analyze photoionization mechanisms.

A solute in a bulk solution is known to photoionize at a lower photon energy than the ionization potential in the gas phase due to neighboring solvent molecules around a solute molecule. However, photoionizing behavior of adsorbed molecules at an aqueous solution surface has hardly studied even though there are a wide variety of surface-active molecules and their adsorption behavior has a great importance in physical chemistry, biochemistry, environmental chemistry, and technology. It seems that the mechanism of photoionization of a molecule at the liquid surface is different from that in the gas phase or in the bulk liquid phase but it has not been clarified due to the lack of precise experimental results.

Furthermore, it is not clarified also how a solute interacts with solvent molecules on photoionization and how much distance from surface the solute molecule participate in that. In this study, photocurrent induced by the single-photon ionization of water-soluble rhodamine dyes is measured at the aqueous solution surfaces using SR. The results are analyzed to determine the photoionization thresholds. The photoionization process and the state of these rhodamine dye molecules are discussed in connection with results of surface tension measurements.

Experimental

Experimental setup for the measurement of single-photon ionization is shown in Fig. 1. Monochromatized SR from BL1B is irradiated upon a solution surface placed between two plate electrodes in the photon energy range of 4-7 eV. The solution (400 μL) is kept on an aluminum plate so that a high voltage (0.8 kV) is applied between the solution surface and an electron-collecting electrode settled in the gas phase. The cell box is purged with He gas. Photoionization current is measured by a pico-ammeter (Model 617, Keithley). The electrode spacing is 5.5 mm. A relative photon intensity distribution is calibrated by the fluorescence intensity of sodium salicylate coated on an acrylic resin plate with a photomultiplier (1P28, Hamamatsu Photonics). Surface tension of the aqueous solutions is measured by a surface-pressure meter (Model HMB, Kyowakaimen) of the Wilhelmy type. RhB and Rh101 (reagent grade, Nacalai) are used as received. Rh6G is purified by recrystallization. Water is purified by a Milli-Q system (Milli-Q Academic, Millipore). Aqueous solutions with a concentration ranging 0-100 μmol dm^{-3} are prepared. In all measurements, the temperature is controlled at 25±1°C under atmospheric pressure.

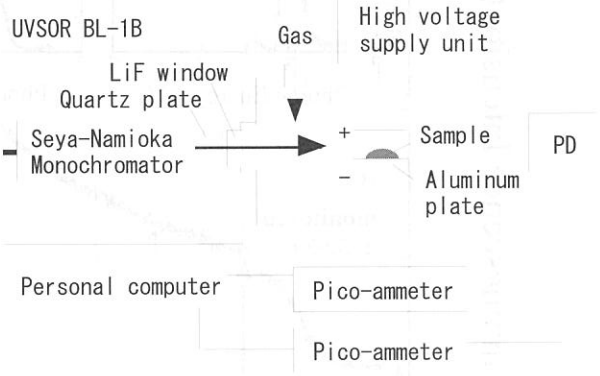

Fig. 1 Schematic diagram of experimental setup for single-photon ionization. PD is the photodetector.

Results and Discussion

Photocurrent spectra at the surface of both pure water and the aqueous solutions of RhB, Rh6G, and Rh101 are shown in Fig. 2, where the photocurrents are normalized with the SR photon intensities. The photocurrent for the surface of pure

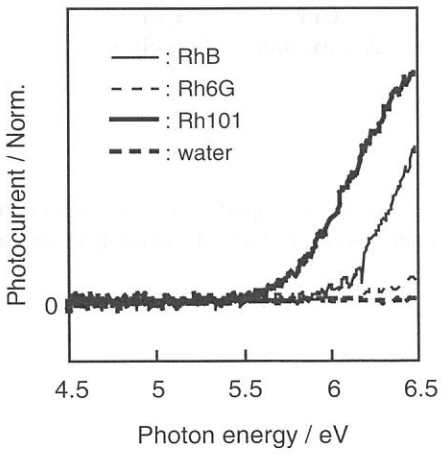

Fig. 2 Photocurrent spectra at the surfaces of pure water and rhodamine aqueous solutions with a concentration of 10 μmol dm^{-3}.

water is not detected in this experimental accuracy. The photocurrents increase with the photon energy above their threshold photon energies. It has been known that the photocurrent, I, near the photoionization threshold, E_{th}, is expressed with an empirical power law,[2]

$$I = C\,(E_{ex})^{\alpha} = C\,(h\nu - E_{th})^{\alpha}, \qquad (1)$$

where C is a constant, E_{ex} is the excess energy, and $h\nu$ is the incident photon energy. The values of E_{th} for rhodamine dyes at the aqueous solution surfaces are determined by fitting Eq. (1) with the exponent $\alpha = 2.5$ to the curves in Fig. 2. A plot of the 0.4 power of the photocurrent vs the photon energy is on a straight line. The values of E_{th} for RhB, Rh6G and Rh101 are determined to be 5.6, 5.6 and 5.3 eV, respectively. The photoionization threshold of a solute in a bulk solution can be related to the ionization potential in the gas phase, IP,

$$E_{th} = IP + P^{+} + V_0, \qquad (2)$$

where P^{+} is the polarization energy of the resultant positive ion and V_0 is the electron affinity in the solvent. Timoshenko et al. derived the value of IP for RhB to be 6.7 eV.[3] Assuming that V_0 in Eq. (2) at the surface is negligible, we can estimate the value of P^{+} at the aqueous solution surface from IP and the obtained photoionization threshold. The value of P^{+} for RhB at the aqueous solution surface is calculated to be –1.1 eV, which is larger than that value in bulk solution estimated from the Born's equation (–0.5 eV).[4] It suggests that probed molecules by single-photon ionization measurements are positioned at a depth from the surface where the resultant positive ion sufficiently interacts with solvent water molecules, and that the value of V_0 cannot be negligible even for molecules at the water surface.

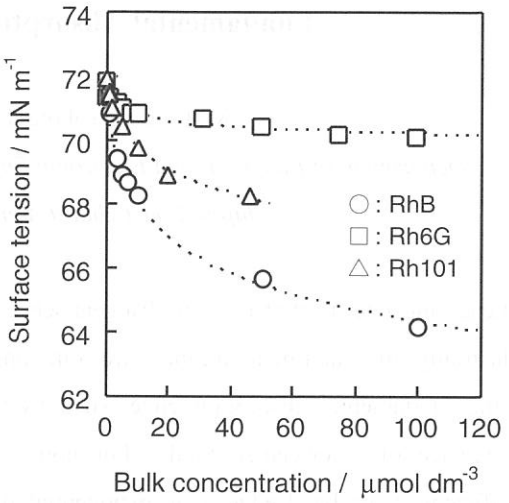

Fig. 3 Bulk concentration dependence of surface tension of the rhodamine aqueous solutions.

Table 1 Experimental results for threshold, signal intensity and surface excess. Concentration of the solutions is 10 μmol dm^{-3}.

Sample	Threshold / eV	Signal intensity / arb. units	Surface excess / μmol m^{-2}
RhB	5.6	1	0.20
Rh6G	5.6	0.16	0.05
Rh101	5.3	2.7	0.13

To discuss the relation between the signal intensity and the amount of solute molecules at the surface, it is necessary to know the number density of rhodamine molecules at the aqueous solution surface. Surface tension measurements are known to be useful for its purpose and the dependence of the surface tension of the rhodamine solutions on their bulk concentration were measured and the result is shown in Fig. 3. Surface tension of each rhodamine aqueous solution decreases with the bulk concentration, which indicates that each rhodamine molecule is adsorbed positively to the surface. The surface excess of each rhodamine molecule can be deduced by applying the thermodynamic equations for the data in Fig. 3 and the result at a 10 μM dye concentration is listed in Table 1 as well as the photoionization threshold and the signal intensity at 6.2 eV. The signal intensity difference between Rh6G and RhB can be regarded as the difference in the surface excess. While, the signal intensity of Rh101 which is much larger than that of RhB despite of smaller surface excess is caused by the difference in the photoionization threshold.

However, there is still a detailed discrepancy in the relation between the surface excess and the photoionization signal intensity. Possible causes of the discrepancy are differences between the rhodamine dyes in photoionization crosssection, direction of the transition moment, depth profile of the molecules and so on. It is important to quantify those values to clarify the cause of the discrepancy though we do not have enough data to discuss them at the present stage and further experiments are now in progress.

References

1. Y. Hatano, *Phys. Rep.-Rev. Sec. Phys. Lett.*, **1999**, *313*, 109.
2. R. A. Holroyd, J. M. Preses, and N. Zevos, *J. Chem. Phys.*, **1983**, *79*, 483.
3. M. M. Timoshenko, I. V. Korkoshko, V. I. Kleimenov, N. E. Petrachenko, Yu. V. Chizhov, V. V. Ryl'kov, and M. E. Akopyan, *Dokl. Phys. Chem.*, **1981**, *260*, 138.
4. M. Born, *Z. Phys.*, **1920**, *1*, 45.

(BL1B)

Fundamental Absorption Edge of $PbWO_4$ Crystals

M. Itoh, H. Yokota, H. Kunisaki, and M. Fujita[A]

Department of Electrical and Electronic Engineering, Shinshu University, Nagano 380-8553

[A]*Japan Coast Guard Academy, Wakaba, Kure 737-8512*

Lead tungstate ($PbWO_4$) is a birefringent scheelite-type crystal consisting of tetragonal unit cell. In this industrially-important material, there are some unresolved problems on optical transmission in the region of the fundamental absorption edge, such as the spectral behavior of the low-energy tail and the appearance of color-center band. For non-metallic solids, it has been found that the absorption coefficient at the band edge is an exponential function of the photon energy at a certain temperature. This dependence is called Urbach rule [1]. Spectral behavior of the fundamental absorption tail in $PbWO_4$ crystals was investigated by Loo [2], who claimed that the Urbach rule does not hold for this material. In the present study, we focus our attention on the low-energy tail of the fundamental absorption of $PbWO_4$.

Single crystals of $PbWO_4$ used in the present experiment were grown by Dr. Usuki. The specimen having a freshly cleaved (011) surface was mounted on the copper holder in a variable-temperature cryostat of He-flow type. Optical transmission measurements were carried out using the ordinary ray ($\boldsymbol{E} \,//\, \boldsymbol{a}$) as a light source.

Figure 1 shows a typical example of the absorption spectra of $PbWO_4$ at $T = 6$ K near the fundamental absorption edge. The results of four crystals cut out of the same or different ingots are presented in this figure. A single absorption band is clearly seen at 3.5 eV for all samples. Its intensity varies from sample to sample. This band is typical of $PbWO_4$ crystal, but the origin is still controversial [3]. The 3.5-eV band overlaps with the tail part of the fundamental absorption. This makes the true shape of the low-energy tail obscure. Fortunately, there is no or little influence of such overlap in the spectrum indicated by asterisk. This spectrum was taken for a crystal with 2.1-mm thickness, the quality of which seems to be the best among the samples investigated.

The absorption coefficients obtained for the best-quality sample at various temperatures are plotted on a logarithmic scale in Fig. 2. The open circles represent the experimental data. The straight lines converge to a point (E_0, α_0), indicating that the Urbach rule certainly holds for $PbWO_4$. From the converging point, we get $E_0 = 4.33$ eV and $\alpha_0 = 4.2 \times 10^7\ \mathrm{cm}^{-1}$. The steepness parameter σ at various temperatures is presented by open circles in Fig. 3. The temperature dependence of σ is expressed as $\sigma(T) = \sigma_0(2k_BT/h\nu)\tanh(h\nu/2k_BT)$. The solid line is the least-squares fit of this equation to the experimental data, with the high-temperature steepness parameter $\sigma_0 = 0.82$ and the average phonon energy $h\nu = 32$ meV.

According to the Sumi-Toyozawa theory [4], the parameter σ_0 is inversely proportional to the strength of the exciton-phonon interaction. The present value $\sigma_0 = 0.82$ is smaller than the critical value (1.50), above which an exciton becomes self-trapped. This fact strongly suggests that the exciton-phonon interaction is strong in $PbWO_4$. In fact, it is known that the intrinsic luminescence of this tungstate appears at 2.80 eV, and is attributed to radiative decay of self-trapped excitons [5].

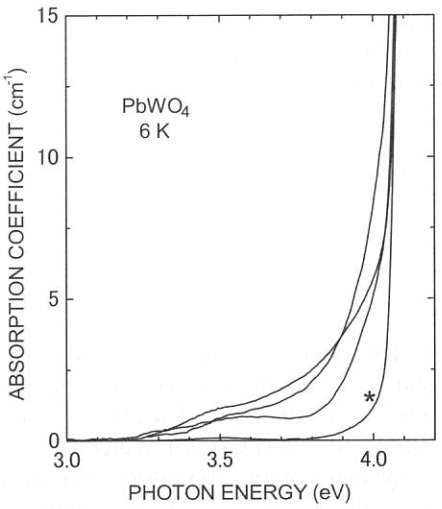

Fig. 1

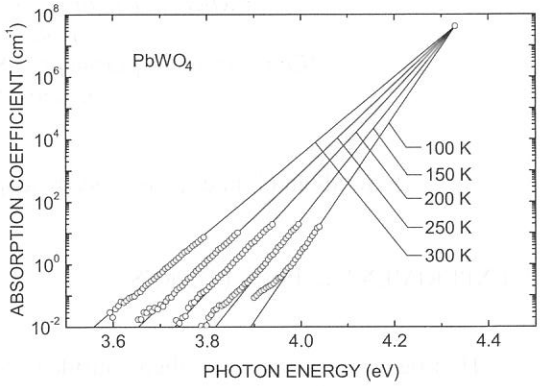

Fig. 2.

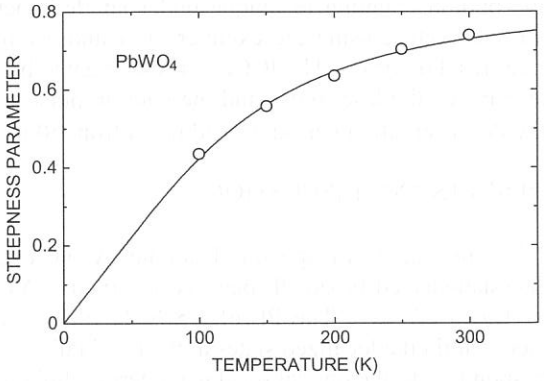

Fig. 3

References

[1] M. V. Kurik: Phys. Status Solidi A **8** (1971) 9.

[2] W. van Loo: Phys. Status Solidi A **27** (1975) 565.

[3] M. Nikl: Phys. Status Solidi A **178** (2000) 595.

[4] H. Sumi and Y. Toyozawa: J. Phys. Soc. Jpn. **31** (1971) 342.

[5] M. Itoh and M. Fujita: Phys. Rev. B **62** (2000) 12825.

(BL1B)

Photoluminescence Properties of Hydrogenated Amorphous Silicon Nitride

Norihide *KASHIO*, Hiromitsu *KATO*, Kwang Soo *SEOL**, Takashi *NOMA*** and Yoshimichi *OHKI*

Department of Electrical, Electronics and Computer Engineering,
Waseda University, 3-4-1, Shinjuku-ku, Tokyo 169-8555.
**RIKEN (The Institute of Physical and Chemical Research),*
Wako-shi, Saitama 351-0198.
***Engineering Department 1, System-LSI Division, Sanyo Electric Co. Ltd.,*
Oizumi-Machi, Gumma 370-0596.

Category 4. Solid- and liquid- phase spectroscopy 1 (IR, VUV, etc)

I. EXPERIMENTAL PROCEDURES

Hydrogenated amorphous silicon nitride (a-SiN_x:H) films were deposited on a silicon monocrystal substrate by plasma-enhanced chemical vapor deposition using SiH_4, NH_3 and N_2 as monomer gases. By increasing the SiH_4 flow rate from 150 to 350 sccm, samples A to C shown in Table I were obtained. The atomic ratio of N to Si, denoted by x, was calculated from XPS spectra obtained with a JEOL JPS-90MX spectrometer.

For PL measurements, two photon sources were used. One is synchrotron radiation (SR) at the BL1B line of UVSOR Facility and the other is a KrF excimer laser with a wavelength of 248 nm (=5.0 eV), a pulse width of 25 ns, and a pulse energy of ~100 mJ/cm^2. Using SR, PL and PL excitation (PLE) spectra were measured at 10 K under multi-bunch operation, while PL decay characteristics were measured at 10 K by a time-correlated single photon counting technique under single-bunch operation. Time-resolved PL spectra were obtained at room temperature using the excimer laser and a monochromator equipped with an intensified charge-coupled device (ICCD) array. The ICCD array was gated by a pulse generator connected to a delay circuit and the delay time between the laser pulse and the gate-on pulse was monitored with an oscilloscope. The gate-on duration or the PL observation period was adjusted from 50 ns to 4 μs so that clear PL spectra could be obtained.

II. RESULTS AND DISCUSSION

Figure 1 shows PL spectra of samples A to C excited by photons with an energy of 5.0 eV from SR at 10 K. A gaussian-shaped broad PL band is observed. As x increases, the PL peak energy shifts to a higher energy from 1.9 to 2.7 eV. The PL of a-SiN_x:H films is considered to be due to recombination of photogenerated carriers within the localized states at the band tails. As shown in Fig. 2, the threshold energy of the PLE spectra, corresponding to the optical band gap energy, shifts to a higher energy with an increase in x. Thus, an increase in the band gap energy is responsible for the blue-shift of the present PL peak. To investigate PL properties further, we have measured time-resolved PL spectra using samples B and C that have stronger PL intensities than sample A. The height of the time-resolved PL spectrum was divided by the gate-on duration, and is shown as a function of the delay time for samples B and C in Fig. 3(a). The PL decays nonexponentially, ranging from ~10^{-8} to 10^{-3} s, which indicates that the PL has a broad lifetime distribution. Therefore, it is convenient to analyze the PL decay by assuming a distribution function $G(\tau)$ of lifetime τ. The distribution function $G(\tau)$ is expressed by the equation,

$$G(\tau)=\text{const}\ I\ (d\log I/d\log \tau), \quad (1)$$

where I is the PL intensity and τ is the lifetime. Figure 3(b) shows the product $\tau G(\tau)$ or the lifetime distribution drawn by choosing $G(\tau)$ so as to yield the best fits to the decay. The lifetime distribution $\tau G(\tau)$ has a component that stretches over a wide range from 10^{-6} to 10^{-3} s. Radiative tunneling recombination is considered to be the main recombination mechanism of this component. In Fig. 3(b), a steep drop in $\tau G(\tau)$ is seen at $\approx 10^{-7}$ s. The PL decay at this early stage was investigated using SR. Figure 4 shows the nanosecond-order decay of PL excited by SR photons with an energy of 5.0 eV, observed in sample B by monitoring at 2.2 eV at 10 K. The decay is nonexponential and can be expressed by a stretched exponential function,

$$I'(t)\propto(\tau'/t)^{1-\beta}\exp[-(t/\tau')^{\beta}], \quad (2)$$

where I' is the PL intensity, t the time, τ' the effective lifetime, and β a parameter that has a value between 0 and 1. The curve in Fig. 4 is the least-squares fit to Eq. (2) of the decay profile. The nanosecond-order decays of the PLs in samples A and C excited by 5.0 eV photons from SR at 10 K were monitored at each excitation peak, namely, at 1.9 eV for sample A and 2.7 eV for sample C. Figure 5 shows the effective lifetime τ' and parameter β, each as a function of x. It is found that τ' increases from 10 to 16 ns with an increase in x, while β is constant at 0.4 independent of x. This fast decay component is considered to be due to an exciton-like recombination. The time-resolved PL and nanosecond-order PL decay measurements indicate that the photogenerated carriers in the band-tail states recombine first through an exciton-like mechanism and then through a radiative tunneling mechanism.

Table I. The ratio of the source gases and N/Si ratio of the a-SiN_x:H films synthesized.

Sample	gas ratio (=NH_3/SiH_4)	x (=N/Si)
A	5.5	0.91
B	7.5	0.97
C	12.5	1.26

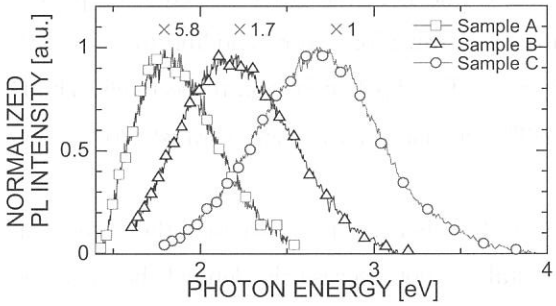

Fig. 1. PL spectra at 10 K observed in samples with different N/Si ratios (x). Numerals beside the spectra are their magnifications.

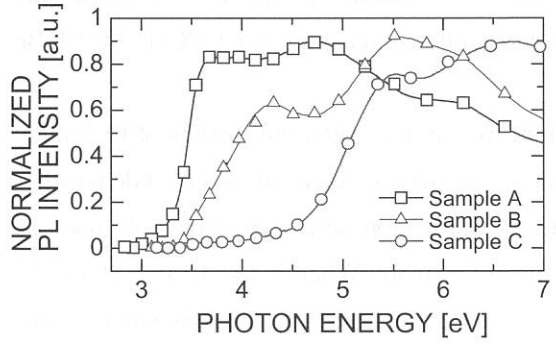

Fig. 2. PLE spectra at 10 K observed in samples with different N/Si ratios (x).

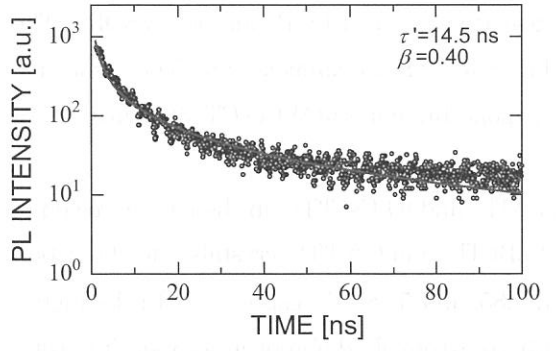

Fig. 4. PL decay at 10 K in sample B monitored at 2.2 eV. Excitaion was done by SR photons with an energy of 5.0 eV.

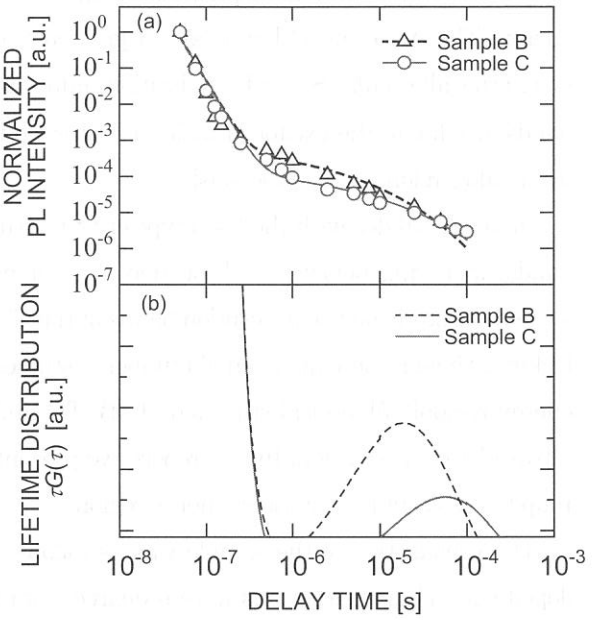

Fig. 3. (a) PL decays and (b) PL lifetime distribution measured in samples B and C, excited by the KrF excimer laser at room temperature. The lifetime distribution stretches over the time range from 10^{-8} to 10^{-3} s.

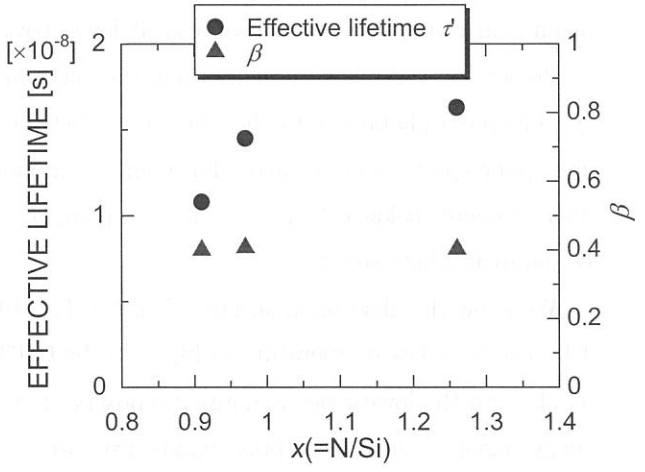

Fig. 5. Effective lifetime τ' and parameter β each as a function of x at 10 K.

(BL1B)

Optical Absorption Bands of Cesium Halides Doped with Tl^+ Ions

Taketoshi KAWAI, and Satoshi HASHIMOTO

Department of Environmental Sciences, Faculty of Science, Osaka Women's University, Daisen-cho, Sakai City, Osaka 590-0035, Japan

It has been well-known that the Tl^+-type centers in alkali halides exhibit several absorption bands in the energy region below the absorption band edge of host crystals. In alkali halides with the NaCl-type crystal structure, these absorption bands are labelled A, B, C and D in the order of increasing photon energy. The A, B and C bands are originated from intraionic transitions corresponding to $^1S_0 \rightarrow {}^3P_1$ (spin-orbit allowed), $^1S_0 \rightarrow {}^3P_2$ (vibration induced) and $^1S_0 \rightarrow {}^1P_1$ (dipole allowed), respectively. The D bands are due to the exciton transition perturbed by the Tl^+-type ions or the charge transfer transition from halogen ions to Tl^+-type ions[1,2].

In alkali halides with the CsCl-type crystal structure, on the other hand, the origin of the absorption bands appearing below the absorption edge of host crystals is not necessarily defined, because the systematic study on the absorption bands of the Tl^+-type centers doped in the CsCl-type alkali halides is lacking. Though there are a small number of studies on CsI:Tl^+ having the absorption bands in the lower energy region[3-5], optical studies on CsBr:Tl^+ and CsCl:Tl^+ are limited[6,7], especially in the vacuum ultraviolet energy region. In this report, we present the optical absorption spectra of CsX:Tl^+ (X=Cl, Br, I) up to the vacuum ultraviolet energy region.

The preparation of the sample was as follows. At first, rapidly quenched bulk ingots of Cs-halides doped with Tl^+ impurity ions were prepared from the melt containing corresponding Tl-halide powders in Cs-halide powders. Next, a small fragment of the ingots was placed on a step of the cell made by putting one smaller quartz or sapphire plate on top of the larger plate. When it was heated above the melting point of the Cs-halides in a nitrogen atmosphere, the melt was percolated into the gap of the cell through capillary action. After infiltrating into a whole area of the cell, thin crystal was grown in the gap by natural cooling. The crystal was cooled down to room temperature within one hour.

For the optical measurements up to the vacuum ultraviolet energy region, the light source was the synchrotron radiation from the 750 MeV electron storage ring at the BL-1B line of UVSOR. The absorption spectra were measured by using a 1 m monochromator of Seya-Namioka type. The absorption measurements below 6.1 eV were made by using a grating monochromator (JASCO CT25CS) attached a D_2 lamp as a light source.

We show the absorption spectra of (a) CsI:Tl^+, (b) CsBr:Tl^+, and (c) CsCl:Tl^+ in the energy region of 4.1～7.8 eV at low temperature in Fig.1. In the CsI:Tl^+, CsBr:Tl^+, and CsCl:Tl^+ crystals, the absorption bands with the lowest peak energy are observed at 4.27, 4.85, and 5.18 eV, respectively. In the higher enegy region, several absorption bands are observed with no extremely different absorption intensity. These absorption bands become close to each other in a sequence of CsCl:Tl^+ → CsBr:Tl^+ → CsI:Tl^+ crystals.

The lowest absorption bands have been assigned to the A absorption bands of the Tl^+-type centers by several authors[3,4,6]. On the other hands, the origin of the higher energy bands has not necessarily been demonstrated. The temperature evolution of the higher energy bands is not characteristic of the Tl^+ centers in NaCl-type alkali halides. From the spectra changes in the $CsBr_{1-x}$ CsI_x : Tl^+ ($0.0 \leqq x \leqq 1.0$) mixed crystals and the temperature dependence of the absorption bands, we assign the higher energy bands to the charger transfer or perturbed exciton transition bands[8]. The B and C bands are not given in our assignment. The difference of the absorption bands between the CsCl-type and NaCl-type alkali halides may be explained in terms of the ion arrangements around the Tl^+ ion. To clear up this problem, further studies of optical transitions in the CsCl-type ionic crystals doped with the Tl^+-type ions are needed.

References

[1] A. Ranfagni, D. Mugnai, M. Bacci, G. Viliani, and M. P. Fontana: Advances in Physics 32 (1983) 823.

[2] P. W. M. Jacobs: J. Phys. Chem. Solids 52 (1991) 35.

[3] K. Asami, T. Naka, and M. Ishiguro : phys. stat. sol. (b) 104 (1981) 145.

[4] M. J. Stillman, P. W. M. Jacobs, K. Oyama Gannon, and D. J. Simkin : phys. stat. sol. (b) 124 (1984) 261.

[5] V. Nagirnyi, A. Stolovich, S. Zazubovich, V. Zeplin, E. Mihokova, M. Nikl, G. P. Pazzi, and L. Salvini: J. Phys. : Condensed Matter 7 (1995) 3637.

[6] V. Nagirnyi, S. Zazubovich, and N. Jaanson: phys. stat. sol. (b) 175 (1993) 155.

[7] E. Mihokova, V. Nagirnyi, M. Nikl, A. Stolovich, G. P. Pazzi, S. Zazubovich, and V. Zeplin: J. Phys. : Condensed Matter 8 (1996) 4301.

[8] T. Kawai, N. Ichimura, and S. Hashimoto: phys. stat. sol. (b) 277 (2001) 587.

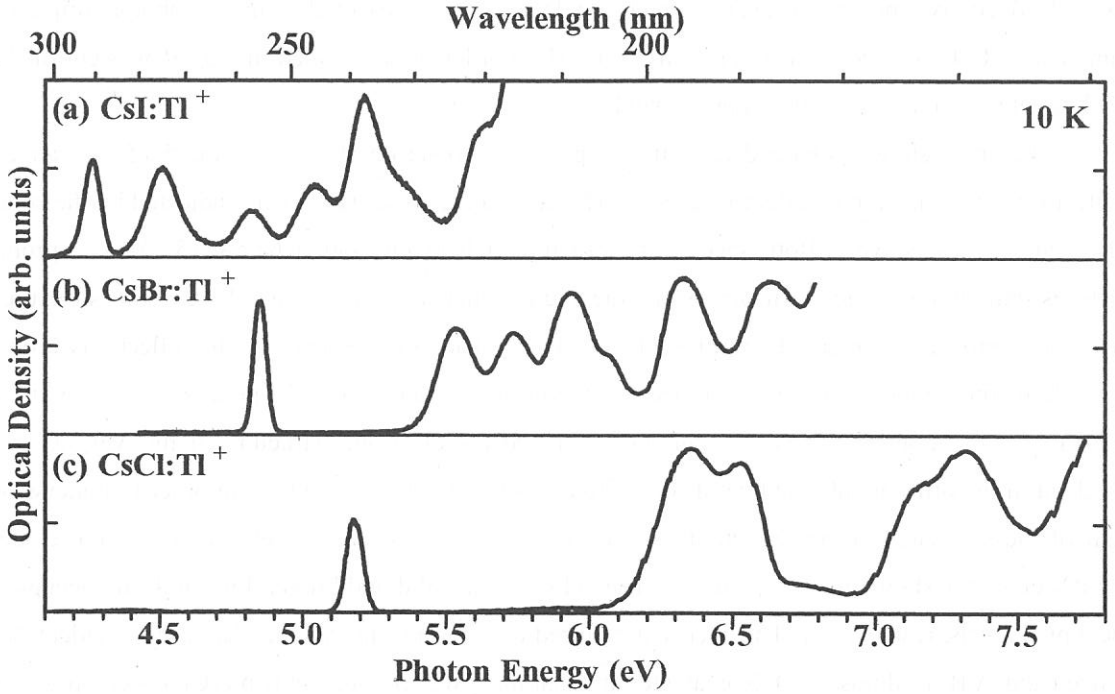

Figure 1 Absorption spectra in Cs-halides doped with Tl^+ centers

(BL-1B)

Reflection Spectra and Electronic Structure of Forsterite (Mg_2SiO_4) Single Crystals

Mamoru KITAURA[A], Hideyuki NAKAGAWA[B] and Akimasa OHNISHI[C]

[A]*Fukui National College of Technology, Sabae 918-8057*

[B]*Department of Electric and Electronics Engineering, Fukui University, Fukui 910-8057*

[C]*Department of Physics, Yamagata University, Yamagata 990-8560*

Magnesium silicate, Mg_2SiO_4, is one of the silicate minerals which make up the majority of the earth's crust and mantle. This material takes two kinds of crystal phases: forsterite with olivine structure, and ringwoodite with spinel structure. They have been studied from the interest in geophysics and crystal chemistry. The electronic structure of forsterite has been investigated by X-ray emission and photoelectron spectroscopy [1]. As far as we know, there is no report on the electronic structure of forsterite except this investigation. In the present study, polarized reflection spectra of forsterite have been measured using synchrotron radiation, in order to obtain the information on its electronic structure. The results obtained here will be applicable to predict the structure, physical and chemical properties of forsterite under ultra-high pressures in the earth's deep interior.

The crystals of forsterite were grown in air by a floating zone (FZ) technique. The orientation of crystal samples was determined by the X-ray analysis. The crystal samples were mounted on a Cu holder of a He-flow-type cryostat. The present experiments were carried out at BL-1B of UVSOR facility. The synchrotron radiation (SR) dispersed with a 1-m Seya-Namioka monochromator was used as a light source. The spectral bandwidth of the SR was fixed to 0.1 nm. The electric vector of the SR is perpendicular to the *b*-axis. Reflectivity spectra of near normal incidence were measured using a photomultiplier tube (Hamamatsu R105) coated with sodium salycilate. High order light included in the SR was cut off by the LiF plate set up in the front of the sample chamber.

Figure 1 shows polarized reflectivity spectra of forsterite at 10 K in the 5-25 eV range. The spectra for the polarization parallel to the *a*-axis (E || a) and the *c*-axis (E || c) are indicated by the solid and broken curves, respectively. Both spectra are structure rich in the region below 15 eV. The prominent structures exhibit remarkable anisotropy. In the higher energy region above 15 eV, the structures are considerably broad, as compared with those below 15 eV. The rapid decrease in the reflectivity around 20 eV would be due to plasmon excitation, because the plasmon energies for the polarization E || a and E || c are estimated to be about 23 eV. We further calculated the electronic structure of the Mg_9SiO_4 cluster embedded in the orthorhombic lattice of forsterite by using the DV-$X\alpha$ method, in order to understand the origin of the structures in the reflectivity spectra of Fig. 1. The energy level diagram of the embedded Mg_9SiO_4 cluster is shown in Fig. 2. In the left hand side, the solid and broken lines indicate occupied and unoccupied levels, respectively. The energy is referred to the top of the valence band. It is evident that the valence band (VB) is almost of O 2*p* character and that the lower conduction band (CB) is composed of the Mg 3*s* orbital with contribution from the Si 3*s* orbital. Therefore, it is most likely that the optical transitions

in the region near the fundamental gap are attributed to the O $2p$ → Mg $3s$ transitions, which are indeed of allowed type. Although the anisotropy of the structures in the region below 15 eV is not explained at present, they reflect the joint density of states between the VB and the lower CB. In addition, we expect that the transitions from the VB to the Mg $3p$ conduction states take place at around 15 eV. This type of the transitions is essentially forbidden, and thus the structures in the region above 15 eV are not so remarkable, as compared with those below 15 eV.

Reference

1. M. A. Al-Kadier, C. Tolon, D. S. Urch: J. Chem. Soc. Faraday Trans. 80 (1984) 669.

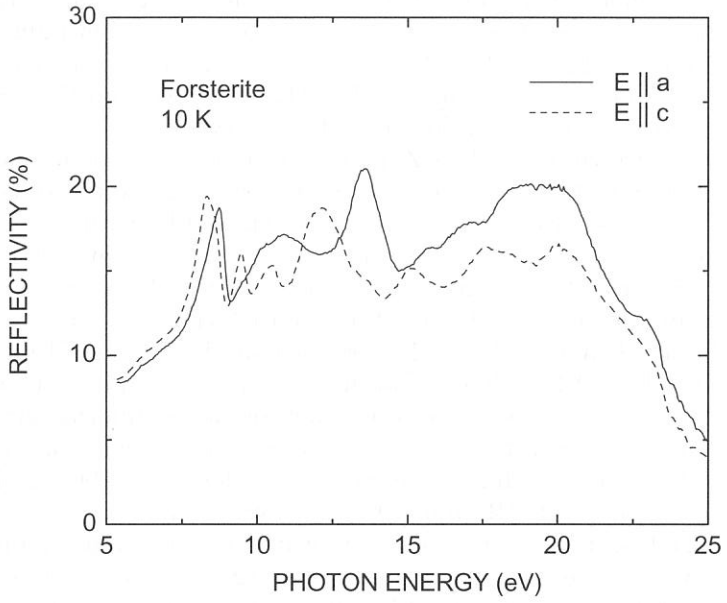

Fig. 1: Polarized reflectivity spectra of forsterite at 10 K in the 5-25 eV range. The spectra were measured for the polarization parallel to the *a*-axis (solid curve) and the *c*-axis (broken curve).

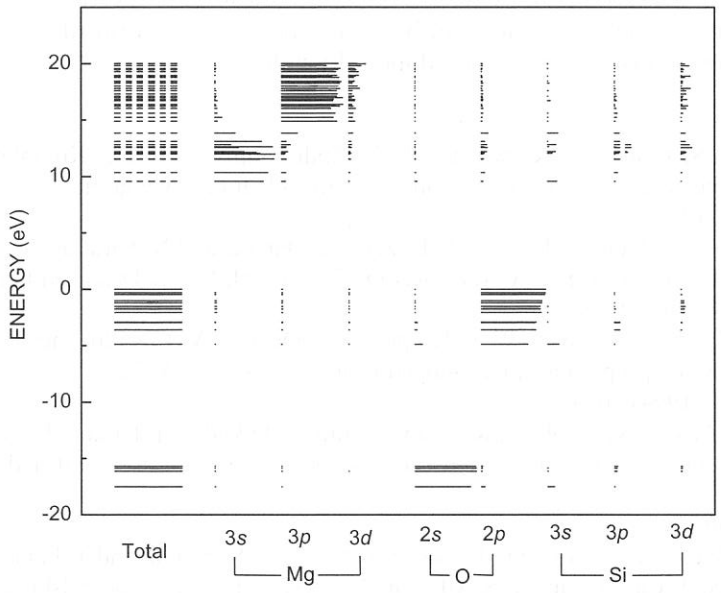

Fig. 2: Energy level diagram of the Mg_9SiO_4 cluster embedded in the orthorhombic lattice of forsterite.

(BL1B)

Observation of New Excitation Channels of Cerium Ion through Absorption by Various Fluoride Host Crystals

Toshimasa Kozeki, Yuji Suzuki, Masahiro Sakai, Hideyuki Ohtake and Nobuhiko Sarukura

Institute for Molecular Science (IMS), Myodaiji, Okazaki 444-8585, Japan

Kiyoshi Shimamura and Tsuguo Fukuda

Tohoku University, 2-1-1 Katahira, Aoba-ku, Sendai 980-8577, Japan

Cerium-ion-doped crystals [1,2] are already known as practical tunable ultraviolet laser media pumped with the fourth harmonic of an Nd:YAG laser. A 60-mJ output from Ce:LiCAF was already demonstrated with large Czochralski (CZ)-grown crystal [3-5], and if other pumping schemes were available, it would expand the applicability of this laser medium. In this paper, we report finding new excitation channels of Cerium ion through Ce:LiCAF, Ce:LiSAF, and Ce:LiSCAF crystals and they coincide completely with the transmission edge of each crystal.

Fluoride crystals were grown using the CZ method. Commercially available AlF_3, CaF_2, SrF_2 and LiF high-purity powders (>99.99 %) were used as the starting material. Growth orientation was controlled by using *a*-axis- oriented seed crystals. The pulling rate was 1 mm/h and the rotation rate was 10 rpm. The growth was carried out in an Ar gas atmosphere and the starting material was melted at 1120 K. Sodium ions were co-doped for the charge compensation.

The transmission, luminescence and excitation characteristics of various fluoride crystals including Ce:LiCAF, Ce:LiSAF, and Ce:LiSCAF were measured using an Ultraviolet Synchrotron Orbital Radiation Facility (UVSOR) with a 1-m focal length Seya-Namioka monochrometer with a photo-multiplier. The luminescence spectrum of Cerium-ion-doped fluoride crystals is known to peak around 290 nm [1]. Therefore, we measured the excitation characteristics of Cerium-ion-doped fluoride crystals with an observation wavelength of 290 nm through band-pass filters. As shown in Fig. 1, the peaks (B) and (C) in the excitation spectrum corresponded to the absorption of Cerium ions. Excitation channels (A) at around 115, 118 and 119 nm for each fluoride crystal coincided roughly with the transmission edges of 112, 118 and 123 nm, respectively. It is interesting that these excitation channels roughly coincide with the bandgaps of each crystal. This result confirmed that these excitation channels can be considered as electrons transfer from the host crystal to the active Cerium ions. A schematic of energy levels and a possible decay channel in the crystal is shown in Fig. 2.

In conclusion, the excitation channels of Cerium ions through fluoride host crystals were observed. These excitation channels indicate the bandgap of the host crystals, and can be used as a potential pumping channel including electron-beam pumping or vacuum ultraviolet pumping, for the future scaling of high-power Cerium-ions-doped fluoride lasers.

References:

[1] M. A. Dubinskii, V. V. Semashko, A. K. Naumov, R. Y. Abdulsabirov, and S. L. Korableva, "Ce^{3+}-doped colquiriite –a new concept of all-solid-state tunable ultraviolet laser," J. Mod. Opt. **40** (1993) 1.

[2] Z. Liu, K. Shimamura, K. Nakano, T. Fukuda, T. Kozeki, H. Ohtake, and N. Sarukura, "High-Pulse-Energy Ultraviolet Ce^{3+}:$LiCAF_6$ Laser Oscillator with Newly Designed Pumping Schemes," Jpn. J. Appl. Phys. **39** (2000) L466.

[3] C. D. Marshall, J. A. Speth, S. A. Payne, W. F. Krupke, G. J. Quarles, V. Castillo, and B. H. T. Chai, "Ultraviolet laser emission properties of Ce^{3+}-doped $LiSrAlF_6$ and $LiCaAlF_6$," J. Opt. Soc. Am. B **11** (1994) 2054.

[4] Z. Liu, T. Kozeki, Y. Suzuki, N. Sarukura, K. Shimamura, T. Fukuda, M. Hirano, H. Hosono "Chirped-pulse amplification of ultraviolet femtosecond pulses by use of Ce^{3+} $LiCaAlF_6$ as a broadband, solid-state gain medium" Opt. Let. **26** (2001) 301.

[5] K. Shimamura, S. L. Baldochi, N. Mujilatu, K. Nakano, Z. Liu, N. Sarukura, and T. Fukuda, "Growth of Ce-doped $LiCaAlF_6$ and $LiSrAlF_6$ single crystals by the Czochralski technique under CF_4 atmosphere,"

J. Crystal Growth **211** (2000) 302.

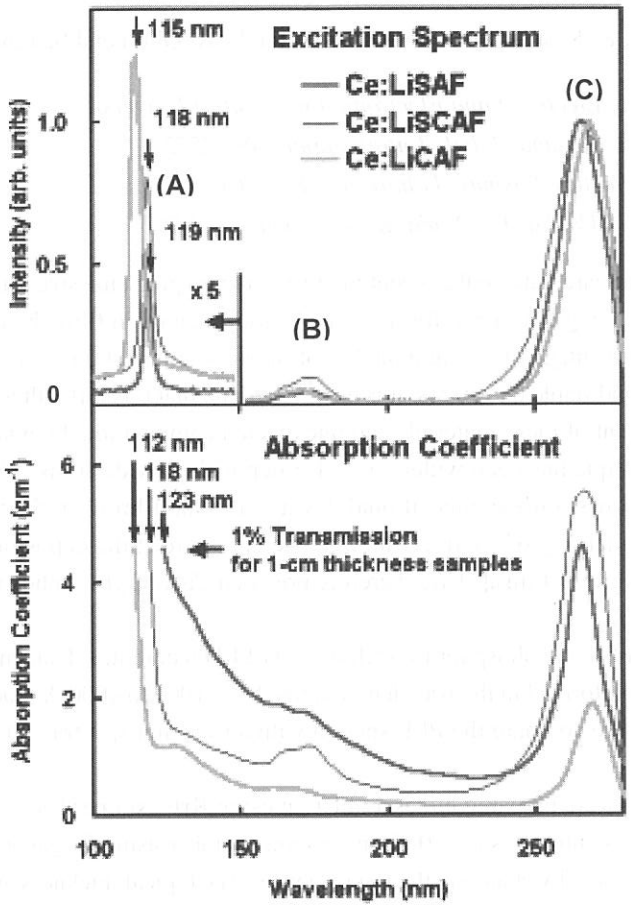

Fig. 1. The excitation spectrum and absorption coefficient curve for Ce:LiCAF, Ce:LiSCAF and Ce:LiSAF crystals.

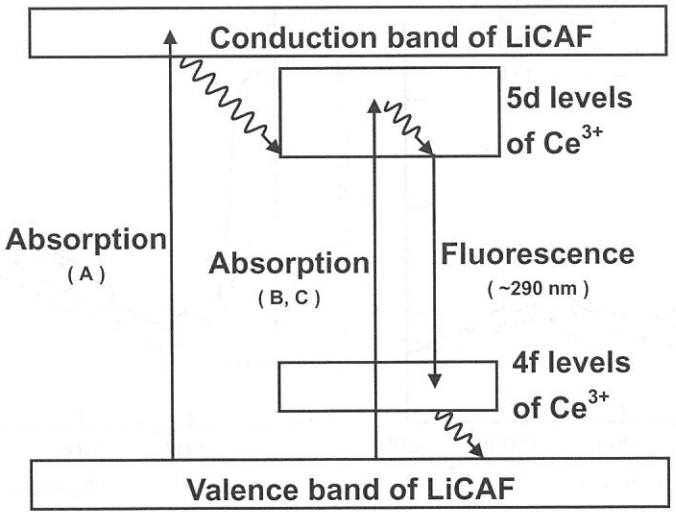

Fig. 2. Schematic of energy levels and possible decay channel in Cerium ions doped crystal.

(BL-1B)

Optical spectra of $CaAl_2O_4:Eu^{2+}$ phosphor thin film prepared by PLD technique

T. Kunimoto*, K. Kakehi, R. Yoshimatsu, S. Honda, K. Ohmi and S. Tanaka

Dept. of Electrical and Electronic Eng., Tottori University
Koyama, 4-101, Tottori, Japan, 680-8552
**Venture Business Laboratory, Kobe Univerisity*
Rokkodai, 1-1, Nada, Kobe, Japan, 657-8501

There is resurgence in phosphor research due to the recent interest in developing emissive flat panel displays. Efficient and stable three-color phosphors are being developed for these applications, and thin film phosphor materials have been attracted much attention due to the advantage of the high quality of pictures. It is well known that oxide phosphor is the promising materials for the efficient and stable phosphors. It is however found that it is difficult to make the complex oxide hosts because of the high melting point of these materials and unexpected compositional deviation.[1] On the contrary, Pulsed laser deposition (PLD) technique has been widely used for depositing oxide films.[2] The advantages for this method include some aspects as follows: little compositional deviation in the film from the target oxide, low growth temperature of substrate, and the availability of relatively high oxygen pressure at the deposition which could facilitate sufficient oxygen incorporation to as-grown films.[3] We therefore prepared $CaAl_2O_4:Eu^{2+}$ phosphor thin films using PLD technique.

We report on the optical spectra of oxide phosphor thin films using PLD technique. Transmission, reflection and PL excitation (PLE) measurement were performed in the wavelength range from 1000 to 4000 Å. Each spectra were corrected by sodium salicylate as a reference. We compare the PLE spectra with absorption spectra and obtain the quantum efficiency for the Eu^{2+} blue emission.

$CaAl_2O_4:Eu^{2+}$ phosphor thin films were prepared by laser ablation using KrF excimer laser (248 nm). The films were deposited on 25×12.5 mm^2 quartz glass substrates at 200 °C in vacuum chamber using O_2 gas injection with 5 sccm flow rate. Obtained films have various thickness by changing the laser fluence. The typical thickness are 500 Å for #29 film and

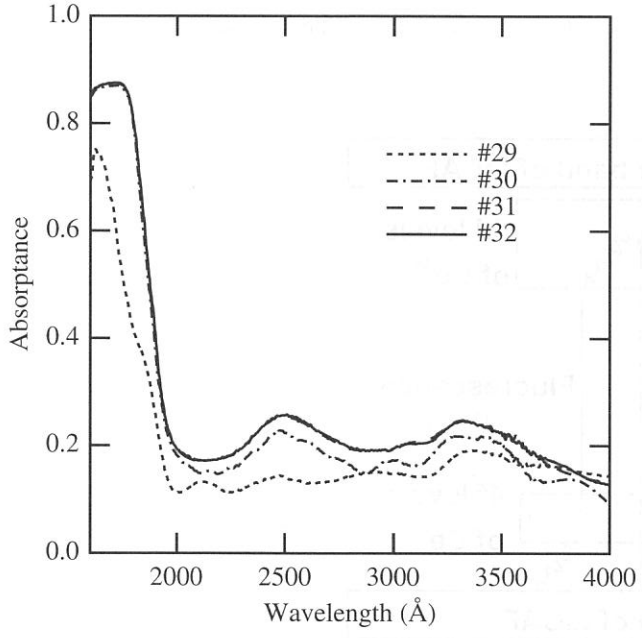

Fig. 1 Absorption spectra of $CaAl_2O_4:Eu^{2+}$ thin films. The films were deposited using various laser fluence (#29 ; 0.5 J/cm^2, #30 ; 1.0J/cm^2, #31 ; 1.5 J/cm^2, #32 ; 2.0 J/cm^2)

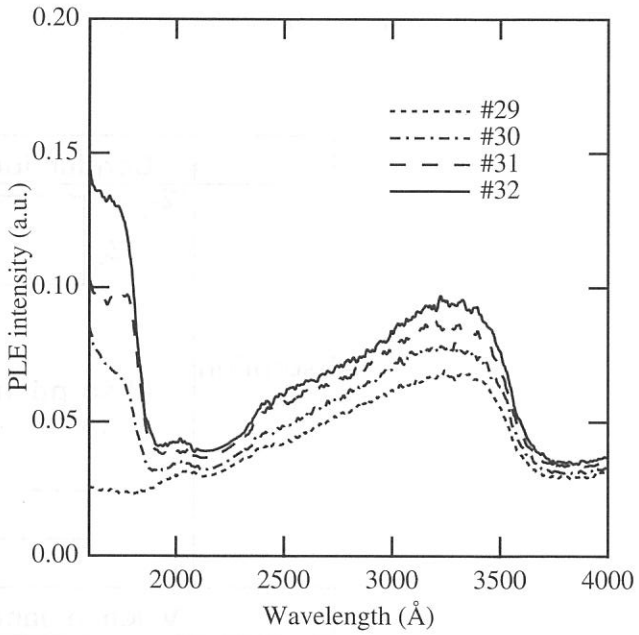

Fig. 2 PL excitation spectra of $CaAl_2O_4:Eu^{2+}$ thin films. The monitor wavelength is 4410 Å.

3000 Å for #32 film. The deposited films crystallized by post-annealing at 950 °C, however the number of diffraction peaks varies with film thickness. The annealed films exhibit the emission band peaking at 4410 Å mainly.

Figure 1 shows the absorption spectra of annealed films. We obtained the absorptance A using following relation,

$$A = 1 - R - T, \quad (1)$$

where T and R are transmittance and reflectance, respectively. The Absorptance increases with increasing the film thickness. The absorption edge structure is observed at 1930 Å and is attributed to the interband transition of host $CaAl_2O_4$. The absorption band observed in the range from 2200 to 3700 Å is associated with the $4f^7$ to $4f^6 5d$ transition of Eu^{2+} ion situated in 9-coordinated Ca(III) site of $CaAl_2O_4$ crystal.

As illustrated in the PLE spectra of Fig. 2, excitation band corresponding to the interband transition of host crystal is observed below 1950 Å, and the direct excitation bands of Eu^{2+} ions are also observed in the range from 2200 to 3600 Å. The position of these excitation bands is consistent with absorption spectrum. The thick thin films (#30, #31, #32) show the relatively strong PLE intensity of the host excitation band. On the contrary the PLE intensity of host excitation band of #29 film is quite weak. The PLE intensity of host excitation band and Eu^{2+} direct excitation bands also increases with increasing the film thickness.

Figure 3 shows the spectral quantum efficiency (QE) of $CaAl_2O_4$:Eu^{2+} phosphor thin films. We obtain QE as following procedure. QE is usually determined by the ratio of the light output and absorptance. The light output is proportional to the measured emission intensity, that is also called PL excitation spectrum $I_{exc}(\lambda)$. In this report, we neglect the wavelength independent factor relating the excitation spectrum to the light output, then QE is finally obtained as

$$QE = I_{exc}(\lambda)/A. \quad (2)$$

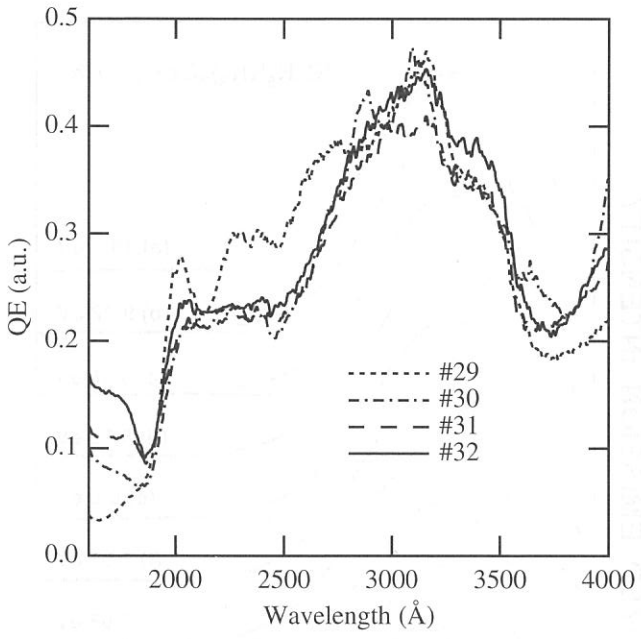

Fig. 3 Quantum efficiency (QE) of $CaAl_2O_4$:Eu^{2+} thin films. QE is determined by the ratio of PLE intensity and absorptance.

As shown in Fig. 3, the QE of Eu^{2+} direct excitation band is relatively high and is almost constant. On the contrary, the QE of host excitation band is quite low and significantly varies with the film thickness. This fact suggests that the migration rate of absorbed energy by host crystal varies with the size of the crystal on the film. Thus, in order to obtain the efficient $CaAl_2O_4$:Eu^{2+} phosphor thin film, it is necessary to increase the size of the crystal.

In summary, Transmission, reflection and PL excitation (PLE) measurement were performed in the wavelength range from 1000 to 4000 Å. We compare the PLE spectra with absorption spectra and obtain the quantum efficiency for the Eu^{2+} blue emission. Quite low QE of host excitation band and its film-thickness dependence are observed.

This work is supported by "Research for the Future Program" through grant JSPS-RFTF 96 R 12501 from "Japan Society for the Promotion of Science" (JSPS).

REFERENCE

[1] C. Sella, J.C. Martin and Y. Charreire: Thin Solid Films **90** (1985) 181.

[2] P. Yu, Z. K. Tang, George K. L. Wong, M. Kawasaki, A. Ohtomo, H. Koinuma and Y. Segawa: Pro. Int. Conf. on the Phys. of Semicond. **2** (1996) 1453.

[3] M. Kawasaki, J. Gong, M. Nantoh, T. Hasegawa, K. Kitazawa, M. Kumagai, K. Hirai, K. Horiguchi, M. Yoshimoto and H. Koinuma: Jpn. J. Appl. Phys. **32**(1993) 1612.

(BL-1B)

Intrinsic Luminescence in $(C_2H_5NH_3)_2CdCl_4$ Single Crystals

[A] Akimasa OHNISHI and [B] Mamoru KITAURA

[A] *Department of Physics, Yamagata University, Yamagata 990-8560*

[B] *Fukui National College of Technology, Sabae 916-8507*

Alkylammonium Cadmium Chloride, $(C_2H_5NH_3)_2CdCl_4$, is a layered ionic crystal of perovskite-type. In the crystal, it has been reported that a largely stokes-shifted luminescence band appears at 2.50 eV under excitation at 5.90 eV into the excitonic absorption region, and at 2.25 eV under excitation at 10.3 eV above the band gap energy. [1] These bands have been supposed to be of intrinsic nature. However, we recently clarified that the lowest exciton absorption band is peaked at 6.19 eV, different from the previous report. [2,3] This finding suggests that the excitation for the intrinsic luminescence occur above 6.19 eV. It is evidence, therefore, that the 2.50 eV band, which is strongly excited in the low energy tail of the lowest exciton absorption, is not intrinsic luminescence. In the present study, recombination luminescence of $(C_2H_5NH_3)_2CdCl_4$ has been investigated in detail under excitation at various photon energies, in order to reconsider the intrinsic luminescence.

$(C_2H_5NH_3)_2CdCl_4$ single crystals were grown at RT by evaporating the aqueous solution containing stoichiometric amounts of $C_2H_5NH_3Cl$ and $CdCl_2$. Samples were cleaved in a plane perpendicular to the *c*-axis, mounted on a Cu holder of a He flow-type cryostat and then were cooled to 7 K. Experiments were performed using synchrotron radiation (SR) from a beam line 1B of UVSOR. Luminescence was analyzed by a Spex 270M monochromator equipped with a CCD detector or a R955 photomultiplier.

Figure 1 shows luminescence spectra of $(C_2H_5NH_3)_2CdCl_4$ measured under excitation at various energies. As shown in Fig. 1(a), a luminescence band is observed at 2.14 eV, when the crystal is excited at 10.8 eV above the

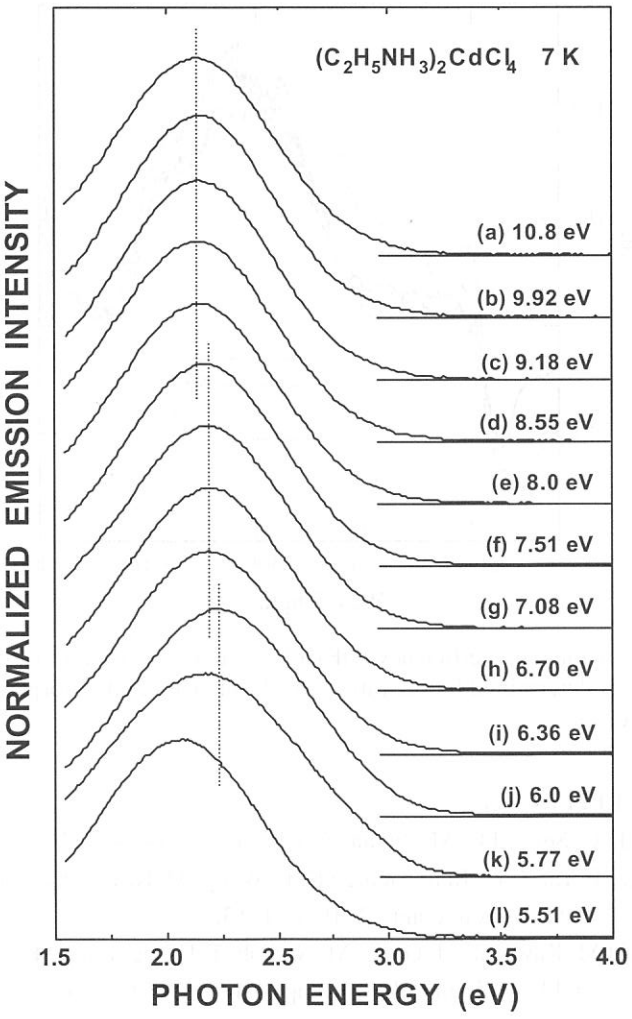

Fig. 1

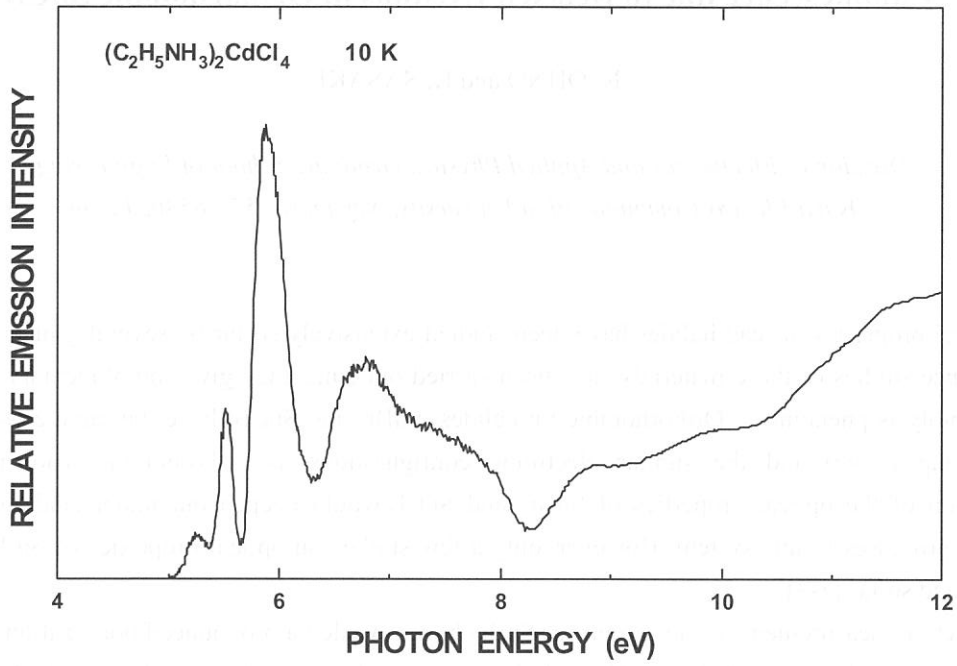

Fig. 2

band gap energy of 6.81 eV. This band appears under excitation above around 8.0 eV (Fig. 1(a) – (e)). In Fig. 2, the excitation spectrum detected at 2.14 eV is shown. The dips at 6.2 eV and 8.2 eV correspond with the peak positions of two kinds of exciton absorption bands, which are due to the transitions from the same Cl *3p* valence band to the conduction bands composed of Cd *5s* and NH_3 *s*-like states, respectively. [2,3] The excitation spectrum indicates high emission yield even below 8.0 eV. When the crystal is excited in the 6.2 – 8.0 eV range, another luminescence band appears at 2.19 eV, as seen in Fig. 1(f) – (i). Thus, the efficiency in the 6.2 – 8.0 eV range is due to the excitation of the 2.19 eV band. On the other hand, it was found that the 2.14 eV and 2.19 eV bands rapidly degrade during prolonged irradiation of excitation lights.

From the results mentioned above, the 2.14 eV and 2.19 eV luminescence bands are undoubtedly assigned to intrinsic luminescence of $(C_2H_5NH_3)_2CdCl_4$. The existence of such two intrinsic luminescence bands suggests that there are two recombination processes of electrons and holes in this crystal. From rapid degradation of their intensities, we speculate that they come from recombination of two kinds of spatially correlated electron-hole pairs.

References

(1) A. Ohnishi, T. Yamada, T. Yoshinari, I. Akimoto, K. Kan'no and T. Kamikawa; J. Electron Spectrosc. Relat. Phenom. **79** (1996) 163.

(2) A. Ohnishi, K. Tanaka, T. Yoshinari: J. Phys. Soc. Jpn. **68** (1999) 288.

(3) A. Ohnishi, K. Tanaka, M. Kitaura, T. Otomo and T. Yoshinari: J. Phys. Soc. Jpn. 70 (2001) 3424.

(BL1B)

Luminescence due to Relaxed Excitons in Orthorhombic $SnCl_2$

N. OHNO and K. SASAKI

Division of Electronics and Applied Physics, Graduate School of Engineering, Osaka Electro-Communication University, Neyagawa 572-8530, Japan

Optical properties of lead halides have been studied extensively so far by several groups. Especially, luminescence studies of these materials have been carried out since they give complimentary information on the photolysis phenomena. Orthorhombic tin halides, $SnBr_2$ and $SnCl_2$, have the same crystal structure (space group *Pmnb*) and the similar electronic configurations as orthorhombic lead halides. The investigation of the optical properties of $SnBr_2$ and $SnCl_2$ would deepen our understanding the energy relaxation processes in this system. However, only a few studies on optical properties of Sn halides have been reported so far [1-3].

Reflection measurements of our group for $SnBr_2$ have revealed a pronounced polarization dependence of the first exciton band at 3.4 eV [4]. The polarization dependence has been well interpreted as a cationic interband transition in Sn^{2+} ($5s \rightarrow 5p$) under the crystal field with C_S symmetry. The logarithmic plot of the fundamental absorption spectra has been found to give a straight line [4], that is, the absorption tail of $SnBr_2$ is well described by the Urbach rule. The obtained small value of the steepness parameter $\sigma_0 = 0.7$ suggests that the electron-phonon interaction is in a strong case in $SnBr_2$, and the free carriers are easily self-trapped. In fact, a luminescence bands with a large Stokes shift was observed under the band-to-band excitation at low temperatures [5,6].

In the present study, reflection and photoluminescence spectra of $SnCl_2$ have been examined at BL1B in the UVSOR facility to obtain the new information on exciton relaxation process in this system. The $SnCl_2$ granule crystals were first purified by distillation in vacuum, and the single crystals were grown by the sublimation method. Figure 1 shows the reflection spectrum up to 12 eV measured at 10 K. One can see a prominent peak at 4.51 eV due to the first exciton transition. The peak energy is almost the same as that reported by Voloshinovskii (4.52 eV at 4.2 K) [3]. There are also seen several sharp peaks at 4.9 and 5.9 eV, and broad peaks in the higher energy region. The structures from 4.5 eV to ~ 9 eV are obviously due to the optical transition from the valence bands. The first exciton transition in $SnCl_2$ is probably ascribed to a cationic interband transition in Sn^{2+} ($5s \rightarrow 5p$) as in the case of $SnBr_2$. However, the optical measurement for polarization dependence is needed to make assignments to the electronic structures in $SnCl_2$.

Figure 2 shows the luminescence and excitation spectra of $SnCl_2$ measured at 10 K. The luminescence spectra are taken under the excitation with 4.13 and 4.48 eV photons. Two luminescence bands peaking at 2.05 and 2.67 eV are observed under the excitation with 4.48 eV photons, while the 2.67 eV band appears under the excitation with 4.13 eV photons. These luminescence bands have a Gaussian lineshape and a large Stokes shift from the lowest exciton energy. The obtained results are almost the same as those reported by Pidzyrailo *et al* [1].

Luminescence excitation spectra were examined for photons emitted at 2.05 and 2.67 eV, respectively. As can be seen in Fig. 2, the 2.05 eV band is stimulated with photons in the low energy region of the first exciton band. On the other hand, the 2.67 eV band is strongly excited with photons in the region of the

lowest exciton band. These excitation spectra exhibit a sharp decrease in intensity as the excitation energy is in the region of the band-to-band transition. The present results suggest that the 2.67 eV band is of intrinsic in origin and is related to the annihilation of self-trapped excitons, and the 2.05 eV band is due to the annihilation of self-tapped excitons perturbed by some impurity.

It is found that the integrated intensity of the 2.67 eV band begins to decrease rapidly at around 30 K, while that of the 2.05 eV band begins to increases at the same temperature. The anti-correlated relation in intensities of these luminescence bands strongly suggests that the self-trapped excitons begin to migrate above 30 K and the exciton energy transfers to the 2.05 eV impurity center.

The authors acknowledge M. Tanaka for her assistance in crystal preparation, optical measurements and data analysis.

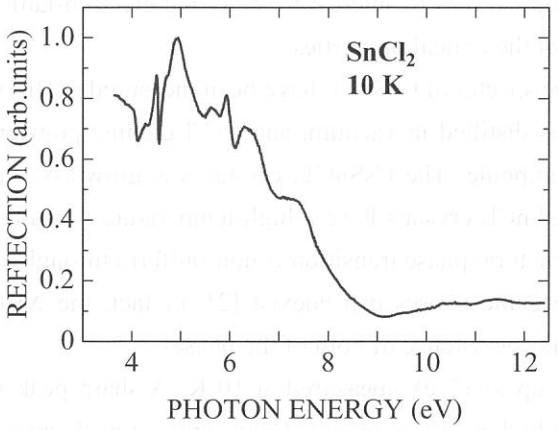

Fig. 1. Reflection spectrum of $SnCl_2$ crystal measured at 10 K.

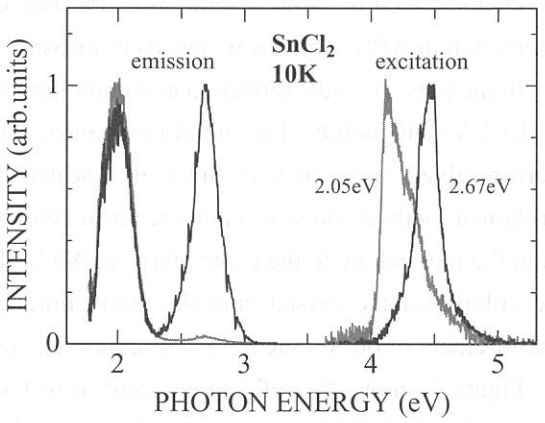

Fig. 2. Luminescence and excitation spectra of $SnCl_2$ measured at 10 K.

References

[1] N.S. Pidzyrailo, A.S. Voloshinovskii, N.G. Stan'ko and Z.A. Khapko: Sov. Phys. Solid State **24** (1982) 708.
[2] A.S. Voloshinovskii, S.V. Myagkota, N.S. Pidsyrailo and Z.A. Khapko: Opt. Spectrosc. **52** (1982) 457.
[3] A.S. Voloshinovskii: Phys. Solid State **35** (1993) 1588.
[4] N. Ohno, Y. Yamasaki, H. Yoshida and M. Fujita: Phys. Status Solidi (b) **223** (2001) 352.
[5] Y. Yamasaki and N. Ohno: UVSOR Activity Report **2000** (2001) 114.
[6] Y. Yamasaki and N. Ohno: Int. J. Mod. Phys. B **15** (2001) 4009

(BL1B)

Photoluminescence of $CsSnCl_3$ Crystal

N. OHNO and K. SASAKI

Division of Electronics and Applied Physics, Graduate School of Engineering, Osaka Electro-Communication University, Neyagawa 572-8530, Japan

The compounds of ABX_3 type (A=Cs, Rb; B=Pb, Sn; X=C1, Br, I) have some interesting optical and electrical properties. For example, free exciton luminescence was found in $CsPbCl_3$ crystal, and $CsSnBr_3$ crystal is of quasi-metal type [1], while $CsSnCl_3$ crystal has dielectric properties. Moreover, these crystals are characterized to show several structural phase transitions. It is of interest to study the electron-lattice interaction in ABX_3 crystals by means of measurements of the optical properties.

In the present study, reflection and photoluminescence spectra of $CsSnCl_3$ have been measured at BL1B in the UVSOR facility. The initial component $SnCl_2$ was distilled in vacuum, and CsCl granule powders were resolved into a melt of $SnCl_2$ in a sealed Pyrex ampoule. The $CsSnC1_3$ crystal was grown by the Bridgman method and was white-cream in color. The $CsSnCl_3$ crystals have a high-temperature transition from the monoclinic to the cubic phase at 390 K. This structural phase transition is non-uniform throughout the volume of the crystal, and the monoclinic and the cubic phases can coexist [2]. In fact, the XRD measurement of our $CsSnCl_3$ crystals exhibited clearly the coexistence of both of the phases.

Figure 1 shows the reflection spectrum of $CsSnC1_3$ up to 12 eV measured at 10 K. A sharp peak is observed at 4.38 eV. There are several broad peaks in the higher energy region. The prominent peak energy is close to the absorption peak of the monoclinic phase reported by Voloshinovskii *et al* (4.0 eV at 77 K) [2], thus it can be assigned as the lowest exciton transition of the monoclinic phase. A small structure is observable at 3.6 eV, which is probably due to the lowest exciton transition of the cubic phase since the absorption peak of the cubic phase is located at 3.5 eV at 77 K [2]. It is to be noted that these lowest exciton energies are almost the same as the first exciton energy of orthorhombic $SnCl_2$ [3,4]. The lowest exciton transitions in $CsSnC1_3$ are ascribed to the cationic interband transition in Sn^{2+} ($5s \rightarrow 5p$) as in $SnCl_2$ [4] and $SnBr_2$ [5].

Luminescence spectra of $CsSnC1_3$ measured at 10 K are shown in Fig. 2. The 2.11 eV band with a full-width at half maximum of 0.26 eV is observed under the excitation with 3.32 eV photons. When the excitation is made with 4.23 eV photons, a luminescence band with an asymmetric lineshape is observed peaking at 2.65 eV. The luminescence excitation spectra for these bands are shown in Fig. 3. The 2.11 eV band is stimulated with photons in the region of the lowest exciton band of the cubic phase, while the 2.67 eV band is strongly excited with photons in the region of the lowest exciton energy of the monoclinic phase. The present results suggest strongly that they are of intrinsic in origin and is related to the annihilation of self-trapped excitons in the respective phases.

It is found that the integrated intensity of the 2.11 eV band begins to decrease at around 40 K, while that of the 2.65 eV band decreases gradually at 20 K and then diminishes at around 50 K. The estimated activation energies using Arrhenius's formula are 37 meV for 2.11 eV band, and 9 and 48 meV for the 2.65 eV band. The two-step thermal quenching of the 2.65 eV band indicates that this luminescence band consists of composite bands.

The authors acknowledge Y. Kitaguchi for her assistance in crystal preparation, optical measurements and data analysis.

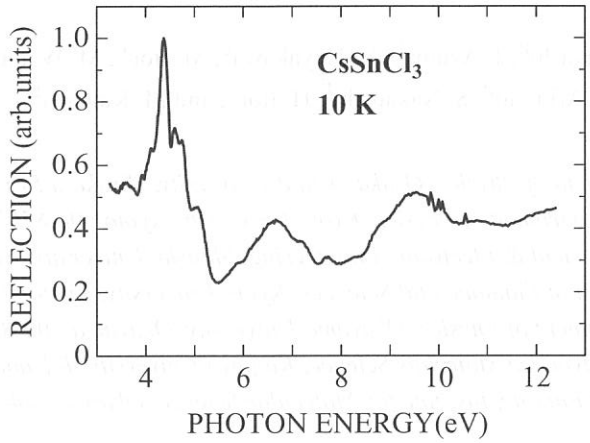

Fig. 1. Reflection spectrum of $CsSnCl_3$ crystal measured at 10 K.

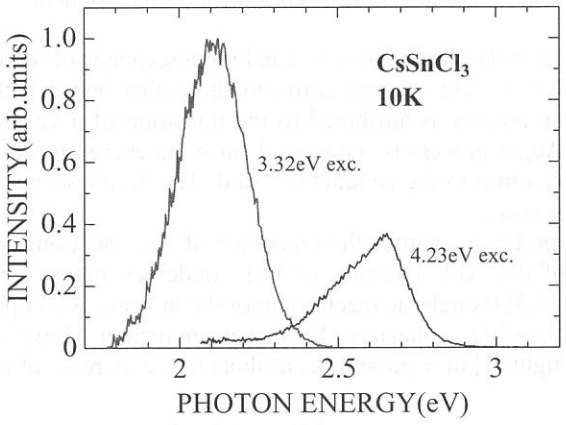

Fig. 2. Luminescence spectra of $CsSnCl_3$ crystal measured at 10 K.

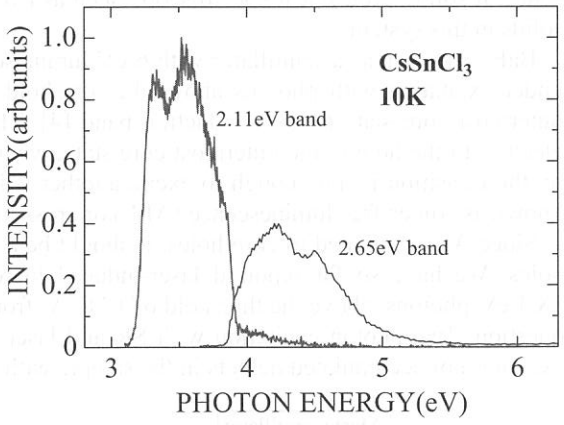

Fig. 3. Excitation spectra of $CsSnCl_3$ crystal measured at 10 K.

References

[1] S. Clark, C. Flint and J. Donaldson, Phys. Chem. Sol. **42** (l981) 133.
[2] A.S. Voloshinovskii, S.V. Myagkota, N.S. Pidzyrailo and M.V. Tokarivskii: J. Appl. Spectrosc. **60** (1994) 226.
[3] A.S. Voloshinovskii: Phys. Solid State **35** (1993) 1588.
[4] N. Ohno and K. Sasaki: UVSOR Activity Report **2001** (2001) in press.
[5] N. Ohno, Y. Yamasaki, H. Yoshida and M. Fujita: Phys. Status Solidi (b) **223** (2001) 352.

(BL1B)

Two-Photon Spectroscopy of Core Electrons in BaF_2 with Synchrotron Radiation and Laser

T. Tsujibayashi[a], J. Azuma[b], K. Hayakawa[c], M. Itoh[c], M. Watanabe[d], O. Arimoto[e], S. Nakanishi[f], H. Itoh[f], and M. Kamada[g]*

[a]*Department of Physics, Osaka Dental University, Hirakata 573-1121*
[b]*Department of Physics, Kyoto University, Kyoto 606-8502*
[c]*Department of Electrical & Electronic Engineering, Shinshu University, Nagano 380-8553*
[d]*Department of Fundamental Sciences, Kyoto University, Kyoto 606-8501*
[e]*Department of Physics, Okayama University, Okayama 700-8530*
[f]*Department of Advanced Materials Science, Kagawa University, Takamatsu 760-8526*
[g]*UVSOR Facility, Institute for Molecular Science, Okazaki 444-8585*

We have been constructing a spectroscopic system in which both synchrotron radiation (SR) and laser are used as light sources [1-3]. A combination of the wide spectral range of SR, from X-ray to infrared, and the high power of lasers is a powerful tool for investigating dynamical behaviors of excitations in inner-shell electronic states of solids. Non-linear spectroscopy such as two-photon and pump-probe spectroscopy can be applicable to solids in this system.

BaF_2 is known as a scintillator with 6-eV luminescence in high-energy physics. The luminescence is observed under excitation with photons above the threshold of 17.8 eV. This energy corresponds to that between the outermost core state to the conduction band [4]. The luminescence is attributed to the transition of a valence electron to the hole in the outermost core state, where an Auger process is suppressed since the energy released by the transition is not enough to excite another valence electron to the conduction band. The luminescence is known as Auger-free luminescence (AFL) or cross luminescence.

Since AFL is related to core holes, it should be a good probe to examine the relaxation of core electrons and holes. We have so far reported laser-induced increase of the AFL intensity of BaF_2 under excitation with 18.4-eV-photons, above the threshold of 17.8 eV, from SR [3,5] though the mechanism of the increase is an open question. Two-photon excitation with SR and laser is a plausible explanation for that phenomenon. However, excitation of accumulated defects in the sample with laser light [6] may possibly contribute to the increase of the

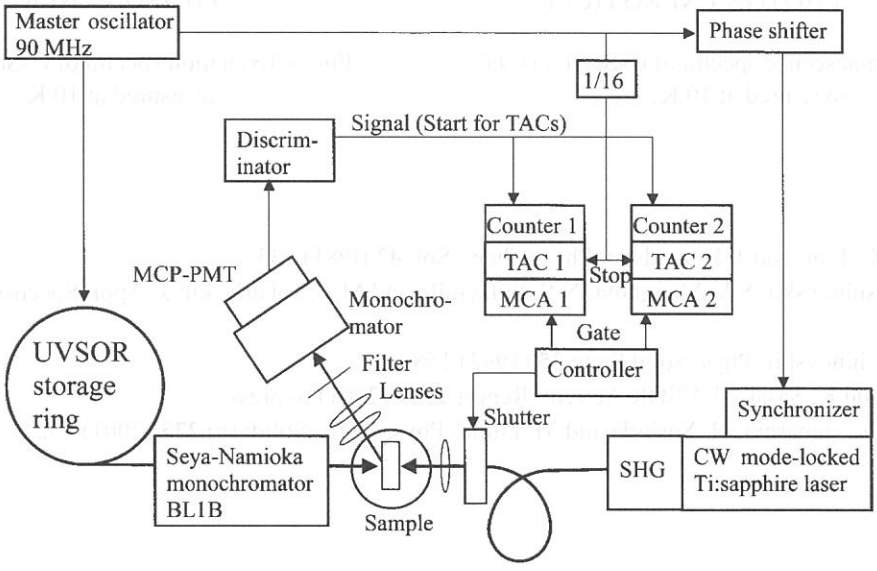

Fig. 1 The block diagram of the experimental setup.

* Present address: *Synchrotron Light Application Research Center, Saga University, 1 Honjyou, Saga 840-9502.*

AFL intensity through changing the branching ratio between decay channels of the core holes. In order to avoid this complexity we lowered the photon-energy of SR below the threshold to 16.7 eV so that AFL is not observed under excitation only with SR. Temporal behavior of the luminescence was measured to clarify whether the luminescence is a consequence of two-photon absorption or not.

The block diagram of the measuring system is depicted in Fig. 1. The laser light was guided to the sample by a 50-m-long optical fiber. The duration of the pulse was stretched from 160 fs to about 0.3 ns during the travel through the fiber. The duration of the laser pulse is comparable to that of the SR pulse under the single bunch operation. The pulse shapes of the laser and SR are shown by solid and broken lines, respectively, in the upper panel of Fig. 2. The temporal behavior of AFL was obtained through the time-correlated single photon counting method. As shown in Fig. 1, MCA1 and MCA2 accumulated the signal when the shutter was open and closed, respectively. The temperature of the sample was kept at 295 K.

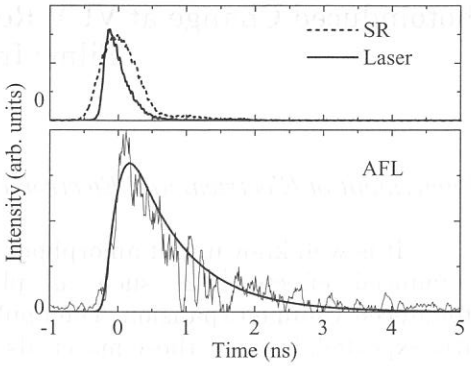

Fig. 2 Upper panel: pulse shapes of SR (broken line) and laser light (solid line). Lower panel: temporal behavior of AFL under excitation with SR (16.7 eV) and laser (3.1 eV). The smooth curve is obtained through convolution analysis (see the text).

The rough curve in the lower panel of Fig. 2 shows temporal behavior of AFL under simultaneous excitation with 16.7-eV-photons of SR and 3.1-eV-photons of the laser. The component of the luminescence caused by scatter and higher harmonics of the Seya-Namioka-type monochromator was eliminated by subtraction of the data on MCA2 (excitation with SR alone) from those on MCA1 (excitation with SR and laser light). We performed convolution analysis of the experimental data. Convoluting the laser pulse shape with an exponentially decaying function was not satisfactory. The smooth curve in the figure was obtained by convoluting the product of SR and laser pulse shapes with an exponentially decaying function with the time constant of 0.8 ns, which is the usual lifetime of AFL. The curve explains the experimental data successfully. This result suggests that the luminescence originates from two-photon absorption of SR and laser light.

References

[1] S. Asaka *et al.*: Rev. Sci. Instrum. **69** (1998) 1931.
[2] S. Asaka *et al.*: UVSOR Activity Report **26** (1999) 34.
[3] T. Tsujibayashi *et al.*: UVSOR Activity Report **28** (2001) 112.
[4] M. Itoh *et al.*: Solid State Commun. **65** (1988) 523.
[5] J. Azuma *et al.*: Nucl. Instrum. & Methods A **467-8** (2001) 1452.
[6] M. Watanabe *et al.*: UVSOR Activity Report **26** (1999) 66.

(BL5B)

Photoinduced Change at VUV Reflection Spectra of Amorphous Chalcogenide Films Induced by BG Light

Koji HAYASHI

Department of Electrical and Electronic Engineering, Gifu University, Gifu 501-1193, JAPAN

It is well known that amorphous chalcogenide semiconductor materials show a variety of photoinduced effects [1,2] such as photodarkening, photoinduced structural change and photoinduced volume expansion. The application of the amorphous materials to optical devices is greatly expected, because these materials are very sensitive to the light. Among those phenomena, the most prominent phenomenon is the so-called photodarkening, which is a parallel shift of the optical absorption edge to lower energy side after irradiation with light whose energy corresponds to the optical bandgap (bandgap (BG) light). This darkened state is removed by annealing near the glass-transition temperature. The X-ray diffraction [3] and the volume change [4,5] of the films before and after irradiation with BG light suggest that the photodarkening is due to a change of the local structure of the amorphous network. Although a large number of studies have been done on the photoinduced phenomena, there is rarely a photoinduced phenomenon in which the details of the mechanism is clarified. These phenomena were studied by exciting outer core electrons with the irradiation of the visible light with the energy corresponding to the optical bandgap or sub-bandgap. Little attention has been give to photoinduced effects by exciting inner core electrons with the irradiation of higher energy photon. To obtain a wide knowledge of the photoinduced effects, it is necessary to investigate photoinduced phenomena on wide energy region. In the previous reports[6], we reported the photodarkening in amorphous chalcogenide films by the irradiation of the vacuum ultra-violet (VUV) light. In our recent study, we observed interesting photoinduced change in the photoconductivity and the total photoyield of amorphous chalcogenide films by the irradiation of the VUV light and the BG light[7-9]. In this report, we investigate the photoinduced change at the VUV reflection spectra of amorphous chalcogenide films induced by BG light.

Samples used for the measurement were amorphous chalcogenide (a-As_2Se_3 and a-As_2S_3) films. Thin films of amorphous chalcogenide were prepared onto quartz substrates by conventional evaporation technique. A typical thickness of an amorphous film was around 0.7 μ m. After evaporation, samples were annealed near the glass transition temperature for two hours in a vacuum with a pressure of 10^{-4} Pa. A xenon arc lamp or a high pressure mercury lamp with IR-cut-off filter were used as a light source. Before the measurement of the VUV reflection spectra, half area of the sample was irradiated with the BG light to the degree in which the sample sufficiently produced the photodarkening. The measurement of the VUV reflection spectra was performed at room temperature at the BL5B beam line of the UVSOR facility of the Institute for Molecular Science. For the measurement of the reflection spectra, the incident angle was near normal to the sample surface and the reflectivity was measured by a silicon photodiode. We also monitored the spectrum of light source by measuring the photoyield of the gold mesh. The reflection spectra were obtained by normalizing the spectra by the spectrometer system response.

Figure 1 shows the VUV reflection spectra of a-As_2S_3 film at room temperature in the photon energy region between 42eV and 50eV. One main peak was observed in this energy region. This peak around 44eV corresponds to the 3d core level of As atom. It can be seen in the figure that the peak of the spectrum observed from the area which irradiated with BG light slightly shifts toward the low energy side and the FWHM becomes narrower as compared to the spectrum observed from the area which dose not irradiate with BG light. It seems to relate these spectral change to the structural change induced by irradiation with BG light. As for the origins of the spectral change, it is not clear. Further analysis of these spectra is now in progress. We also investigate the photoinduced change at the spectra of a-As_2Se_3 films. Method for accurately measuring the peak position and for removing the effect of the higher order light are examined at present. The detailed experiments and analysis will be done in the next step.

This work was partly supported by grants-in-aid for Scientific Research from the Ministry of Education, Science and Culture of Japan.

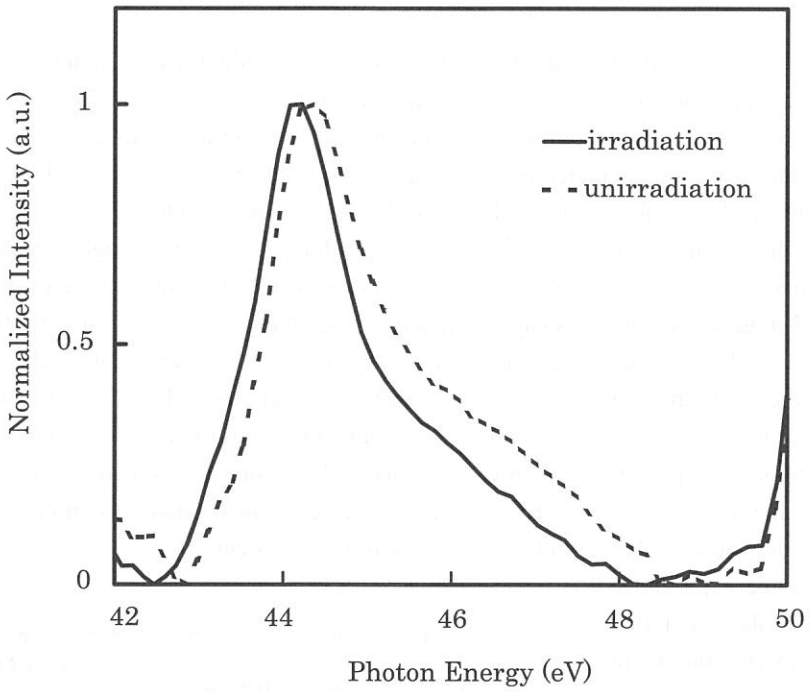

Fig. 1. VUV reflection spectra of a-As_2S_3 film at room temperature in irradiation area (solid line) and unirradiation area (broken line) of BG light.

REFERENCES

[1] Ke. Tanaka, Rev. Solid State Sci., 4(1990)641.
[2] K. Shimakawa, A. Kolobov, and S. R. Elliott, Adv. Phys., 44(1995)475.
[3] Ka. Tanaka: Fundamental Physics of Amorphous Semiconductors, ed. F. Yonezawa, (Springer, Berlin, 1981), p.104.
[4] Ka. Tanaka: Proc. A.I.P. Conf. Structure and Excitations of Amorphous Solid, ed. G. Lucovsky and G.L. Galeemer, Vol.31, (A.I.P., New York, 1977), p.148.
[5] S. R. Elliott, J. Non-Cryst. Solids, 81(1986)71.
[6] K. Hayashi, D. Kato, and K. Shimakawa, J. Non-Cryst. Solids., 198-200(1996)696.
[7] K. Hayashi, A. Hirai, and K. Shimakawa, UVSOR Activity Report 1996(1997)116.
[8] K. Hayashi, UVSOR Activity Report 1997(1998)118.
[9] K. Hayashi, UVSOR Activity Report 1998(1999)105.

(BL5B), (BL8B1)

Magnetic Kerr Rotation Measurement on Ni around Its $M_{2,3}$ Edges

K. Saito, M. Igeta, T. Ejima, T. Hatano and M. Watanabe

Institute of Multidisciplinary Research for Advanced Materials, Tohoku University
Katahira 2-1-1, Aoba-ku, Sendai 980-8577

In the previous study, we have reported for the first time the longitudinal Kerr rotation measurement on Co around its $M_{2,3}$ edges utilizing the developed magnetic Kerr rotation apparatus in the 50-70 eV at BL5B of the UVSOR facility.[1] The measured longitudinal Kerr rotation angle spectra for angles of incidence of $\theta = 65°$ and $\theta = 80°$ have been compared with the calculated ones from the measured Faraday rotation angle spectrum using the Maxwell-Fresnel approach. It was found that both spectra had the similar spectral shape and θ-dependence of the rotation angle, but the absolute value of the measured longitudinal Kerr rotation angle was larger than that of the calculated one from the Faraday rotation spectrum. The reason was thought to be due to the fact that the magnetic field of 0.82 T generated by the shared permanent magnetic circuit could saturate the magnetization parallel to the Co film plane in the longitudinal Kerr rotation measurement, but could not saturate the magnetization perpendicular to the plane in the Faraday rotation measurement, because the demagnetizing field is strong. In the case of the Ni film, it is expected that the applied magnetic field of 0.82 T is strong enough to saturate the magnetization even perpendicular to the film plane. Therefore in this study, by the use of the same apparatus, the similar measurements on a Ni film were performed, which enable us more direct comparison between the results of the magnetic Kerr and Faraday rotation measurements.

Figure 1 shows, the experimental and calculated results of the longitudinal Kerr rotation angle spectra on 98 nm thick Ni film, for the *s*-polarized incident light at the angle of incidence of $\theta = 65°$. The experimental result is plotted by open circles, and the calculated one, by dashed curve which is obtained through Maxwell-Fresnel approach from the result of the Faraday rotation measurement on a 31.5 nm thick Ni film at BL8B1 of the UVSOR.[2] Each measurement was performed at room temperature. Both spectra are almost the same, as seen in Fig. 1. Therefore, we conclude that the consistency between the magnetic Kerr and Faraday rotation measurements was confirmed directly. Now we are proceeding with the study on magnetic multilayer systems.

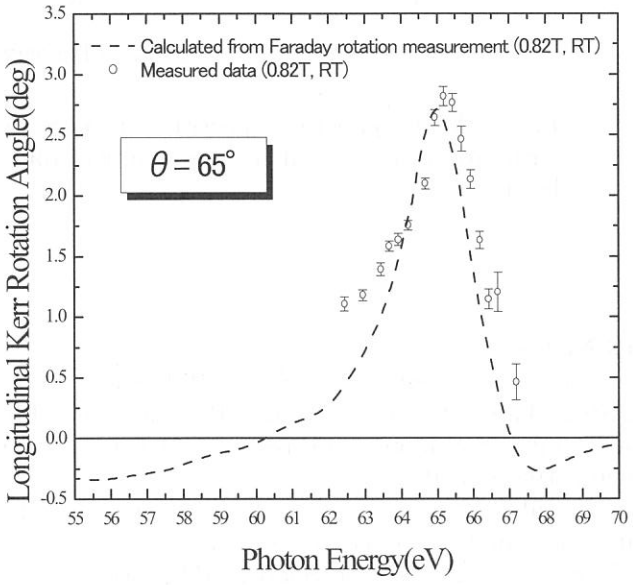

Fig. 1. Longitudinal Kerr rotation angle spectra of 98 nm thick Ni film on Si wafer for *s*-polarized incident light around Ni $M_{2,3}$ absorption edges, at angle of incidence of $\theta = 65°$.

References

1) K. Saito, M. Igeta, T. Ejima, T. Hatano and M. Watanabe, UVSOR Activity Report 2000 (2001) 124.
2) T. Hatano, W. Hu, K. Saito and M. Watanabe, J. Electr. Spectr. Rel. Phenom. **101** (1999) 287.

(BL6A1)

Magneto-Optical Study on Electronic Structure of $Ce_{1-x}La_xSb$ (x = 0, 0.1) in the Infrared Region

S. Kimura[1,2], T. Nishi[1], H. Iwata[1], M. Okuno[1], H. Kitazawa[3] and G. Kido[3]

[1]*Graduate School of Science and Technology, Kobe University, Nada-ku, Kobe 657-8501*
[2]*Japan Science and Technology Corporation*
[3]*National Research Institute for Metals, Tsukuba, 305-0047*

Cerium monoantimonide (CeSb) is a typical strongly correlated semimetal with 4*f* electrons. It has a complex magnetic phase diagram with 16 magnetic phases. [1] The main mechanism is known to be the mixing effect between the Ce 4*f* and the Sb 5*d* states, so-called the *pf* mixing effect. [2] Due to the *pf* mixing effect, the band structure near the Fermi level drastically changes with magnetic phases. The change of the electronic structure has been detected by magneto-optical experiments in the infrared region by us [3] and the other groups [4,5]. The change of the electronic structure produces a large magneto-optical effect because of the strong polarization of the electronic structure. Until now, we revealed the detail mechanism of the strong magneto-optical effect. The main origin is the mixing effect between Sb 5*p* and Ce 5*d* induced by the *pf* mixing (*pf* + *pd* mixing). [6]

In our magnetic circular dichroism measurement of CeSb, a peak was found at 0.4 eV in the $\sigma_+(\omega)$ spectrum in the ferromagnetic phase in contrast to the $\sigma_-(\omega)$ spectrum. According to a theoretical prediction, the peak shifts to the lower energy side in $Ce_{1-x}La_xSb$ ($x > 0$) because the *pf* mixing and also the *pd* mixing are suppressed by the La substitution.

To confirm the theoretical prediction, we measured the magnetic circular dichroism of $Ce_{0.9}La_{0.1}Sb$ in the ferromagnetic phase. Because of the weak *pf* mixing intensity, the ferromagnetic phase appears at lower temperatures than 5 K. Then we made a new cryostat that is a continuous liquid helium flow type and reaches down to 4.0 K for the infrared magneto-optical apparatus at BL6A1.

Figure 1 indicates the magnetic circular dichroism of optical conductivity of $Ce_{0.9}La_{0.1}Sb$ and CeSb in these ferromagnetic phases. The spectral tendency is similar to each other, i.e., the $\sigma_+(\omega)$ is higher (lower) intensity than the $\sigma_-(\omega)$ around 0.4 eV (above 0.6 eV and below 0.25 eV). Since it originates from the polarization of the electronic structure in the ferromagnetic phase, the outline of the electronic structure is similar to each other. The different point of the spectral shape is the peak at 0.35 eV in CeSb shifts to 0.25 eV in $Ce_{0.9}La_{0.1}Sb$. This is considered to originate from the weak *pf* mixing effect as theoretically predicted.

[1] J. Rossat-Mignod *et al.*, J. Magn. Magn. Mater. **52**, 111 (1985).
[2] H. Takahashi and T. Kasuya, J. Phys. C: Solid State Phys. **18**, 2697, 2709, 2721, 2731, 2745, 2755 (1985).
[3] S. Kimura *et al.*, J. Phys. Soc. Jpn. **69**, 647 (2000).
[4] R. Pittini *et al.*, Phys. Rev. Lett. **77**, 944 (1996).
[5] F. Salghetti-Drioli *et al.*, Solid State Commun. **109**, 687 (1999).
[6] F. Ishiyama and O. Sakai, J. Phys.Soc. Jpn. **71** (2002) in press.

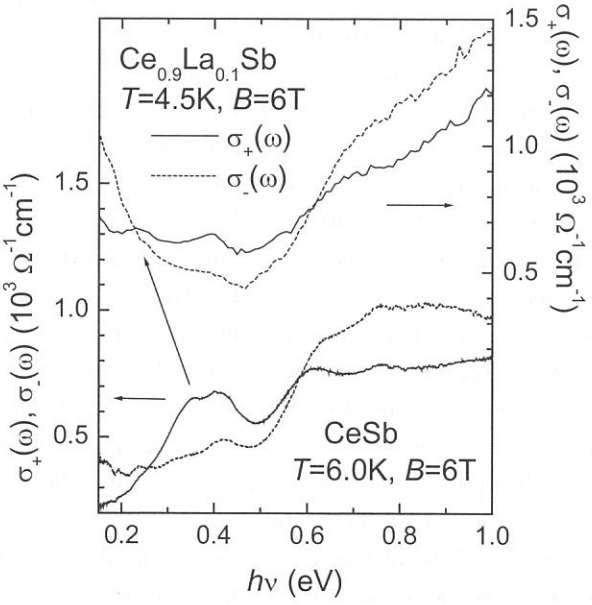

Fig. 1. Magnetic circular dichroism of $Ce_{0.9}La_{0.1}Sb$ and CeSb in the ferromagnetic phase.

(BL6A1)

Far-infrared and Millimeter Wave Spectra of Iodide Doped Silver Phosphate Glass

Teruyoshi AWANO

Department of Applied Physics, Tohoku Gakuin University, Tagajo 985-8537

Enhancement of ionic conductivity by doping of PbI_2 in $AgPO_3$ glass was reported previously[1]. Swenson et al. investigated mechanism of the enhancement on the PbI_2-$AgPO_3$ glass by diffraction measurements and reverse Monte Carlo simulation[2]. They explained the increase of ionic conductivity by that the doped Pb^{2+} substitute Ag^+ which is connected with non-bonding oxygen and the released Ag^+ contribute to ionic conduction. The doped I^- extend space between PO_4 chains and conduction channel for Ag^+ is expanded.

The enhancement of ionic conductivity by metal iodide doping has also been reported on BiI_3 and CdI_2 and NaI[3]. The increase of ionic conductivity is proportional to dopant concentration and valence of the metal ion. This paper reports results of far-infrared and millimeter wave spectra of BiI_3-$AgPO_3$ and CdI_2-$AgPO_3$ glasses to investigate the effect of valence numbers of cations on the enhancement of ionic conductivity.

BiI_3 or CdI_2 doped $AgPO_3$ glasses were obtained by quenching melt of product after reaction of $NH_4H_2PO_4$, $AgNO_3$ and BiI_3 or CdI_2 at 400℃ for two hours after pre-heating at 200℃ for 12 hours. Far-infrared and millimeter wave reflectivity spectra were measured by SPECAC Murtin-Puplett interferometer. Optical constants were obtained by Kramers-Kronig analysis.

Fig. 1 shows reflectivity spectra of $AgPO_3$, $(BiI_3)_{0.05}(AgPO_3)_{0.95}$ and $(CdI_2)_{0.05}(AgPO_3)_{0.95}$ glasses. Dotted line shows the reflectivity of pure silver phosphate glass. Solid and dashed line shows that of BiI_3 or CdI_2 doped glass respectively. Intensity change was observed at 100 cm^{-1} peak in the doped glasses. Fig. 2 shows absorption spectra obtained by Kramers-Kronig analysis from the reflectivity spectra. The reflectivity was extrapolated as constant at lower and higher energy region than the measured one. Absorption peaks were observed at 550, 460, 350 and 125 cm^{-1} in $(BiI_3)_{0.1}(AgPO_3)_{0.9}$ glass. Former three peaks, which are assigned as bending and torsional modes of PO_4 unit[4, 5], were observed at the same positions and at the same intensities as those in $AgPO_3$ glass, although the last peak was located at lower position and at more strength than in $AgPO_3$, in which the Ag-O vibration absorption is at 133 cm^{-1} as shown in fig. 3, which is the magnified one of fig. 2. In $(CdI_2)_{0.1}(AgPO_3)_{0.9}$, the peak was at 129 cm^{-1} and the position shift were little than that of $(BiI_3)_{0.05}(AgPO_3)_{0.95}$, although the strength is more than that in $AgPO_3$ as shown in fig. 3. Other peaks in $(CdI_2)_{0.1}(AgPO_3)_{0.9}$ were at the same positions as those in $AgPO_3$ as shown in fig.2. The shift of the 125 cm^{-1} peak in $(BiI_3)_{0.1}(AgPO_3)_{0.9}$ glass from that in $AgPO_3$ seems to be due to the following mechanism.

A part of silver ions in $AgPO_3$ are replaced by bismuth ions in $(BiI_3)_{0.1}(AgPO_3)_{0.9}$ because the doped Bi^{3+} couples by covalent bond with a nonbonding oxygen. Therefore the intensity of Ag-O vibration decreases as shown by dashed line in fig. 3. The Gaussian curve was drown as the intensity decreased 15 percent in $(BiI_3)_{0.05}(AgPO_3)_{0.95}$ because one doped Bi^{3+} ion must alternates three Ag^+ ions for the charge neutrality. The released Ag^+ ions couple with iodine ions and Ag-I vibrational absorption band grows as at 115 cm^{-1} as shown in the figure. The intensity of the absorption band is drown as 30 percent of the 133 cm^{-1} band in $AgPO_3$. This ratio should be 15 percent in this model. This difference seems to be due to the difference of the strength of oscillator. Bi-O absorption band of the intensity of 5 percent of original Ag-O band is

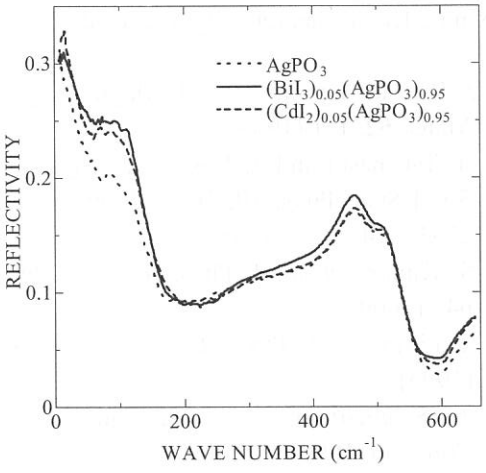

Fig. 1. Reflectivity spectra of pure and doped silver phosphate glasses.

also drawn at 150 cm^{-1} [4] in the figure. Net absorption spectrum by these spectral change is shown by thick solid line. This simulation spectrum agrees with the observed one around 100 cm^{-1}. In $(CdI_2)_{0.1}(AgPO_3)_{0.9}$, the peek shift was smaller than that of $(BiI_3)_{0.05}(AgPO_3)_{0.95}$. This seems to be due to that Cd-O vibrational frequency is almost the same as that of Ag-O [4], because the mass of cadmium ion is almost the same as that of silver ion. The changeless of three absorption bands shows that the glass network structure itself is not affected by the metal doping.

The far-infrared spectral change showed the mechanism of the enhancement of ionic conductivity in BiI_3-$AgPO_3$ and CdI_2-$AgPO_3$ glasses. A doped metal ion substitutes a silver ion which is connected with a nonbonding oxygen. The released silver ion is coordinated weakly with an iodine ion and conducts easily. This mechanism are the same as that in PbI_2-$AgPO_3$ glass.

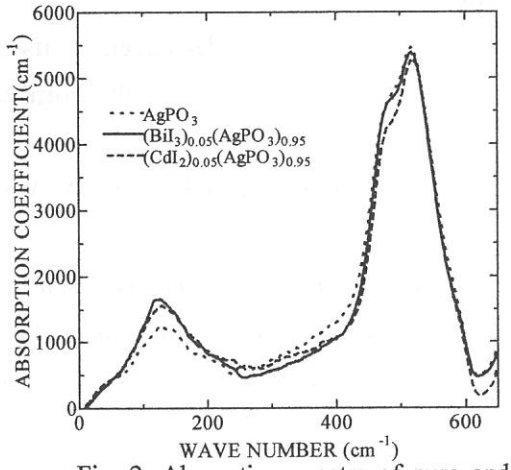

Fig. 2. Absorption spectra of pure and doped silver phosphate glasses obtained from the reflectivity spectra by Kramers- Kronig analysis.

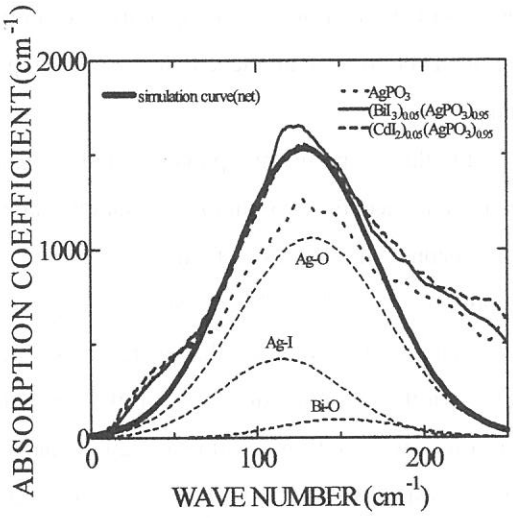

Fig. 3. Magnified spectra of fig. 2 and simulation curves of Ag-O, Ag-I, Bi-O vibration absorption and the net curve of them.

REFERENCES

[1] J. P. Malugani, R. Mercier and M. Tachez, Solid State Ionics, 21 (1986) 131.

[2] J. Swenson, A. Matic, C. Gejke, L. Boerjesson, W. S. Howells and M. J. Capitan, Phys. Rev. B60 (1999) 12023.

[3] H. Nakajin, H. Takahashi and T. Sakuma, Annual meeting of the Physical Society of Japan 1999, 31a-ZE-10.

[4] B. N. Nelson and G. J. Exarhos, J. Chem. Phys. ,71 (1979) 2739.

[5] K. Wakamura, J. Katagi and H. Takahashi, Physica B263-264 (1999) 799.

(BL6A1)

Infrared transient absorption obtained from the combined laser-SR experiment

J. Azuma, M. Iwanaga[A], M. Watanabe[B], M. Kitaura[C], M. Itoh[D] and M. Kamada[E]

Dept. of Phys., Kyoto Univ., Graduate school of Human and Environmental Studies, Kyoto Univ.[A], *Faculty of Integrated Human Studies, Kyoto Univ.*[B], *Fukui National College of Technology*[C], *Faculty of Engineering, Shinshu Univ.*[D], *UVSOR, Institute for Molecular Science*[E]

Transient absorption measurement is a powerful technique to investigate the photo-excited states in condensed matters. Some important results have been obtained by this technique in the visible region[1,2]. It is necessary to expand the spectral range to the infrared (IR) region in order to apply to other interesting topics which cannot be studied in the usual technique in the visible region[3]. It is well known that synchrotron radiation (SR) is a brilliant light source not only in the X-ray or vacuum ultra violet region but also in the IR region. Therefore we are developing the technique of the infrared transient absorption measurement by using SR and laser.

In this experiment, photo-excited states were generated by two-photon excitation using the second harmonics of the regenerative amplified Ti:sapphire laser (Spectra Physics, Hurricane). The wavelength, average power, pulse width and repetition rate of the second harmonics were 400 nm, 250 mW, 120 fs, and 1 KHz, respectively. The measurement was performed in the energy range of 80～13000 cm^{-1} with the rapid-scan Michelson interferometer (Bruker, IFS-66V) by using quartz, KBr and mylar beam splitters. A HgCdTe detector and a Si borometer were used for the energy range of 400～13000 cm^{-1} and 80～500 cm^{-1}, respectively. The transient absorption was obtained from the difference between the transmitted IR intensities with and without the laser excitation. The single crystal of lead bromide was used as a sample in this experiment.

In lead halides, it has been strongly

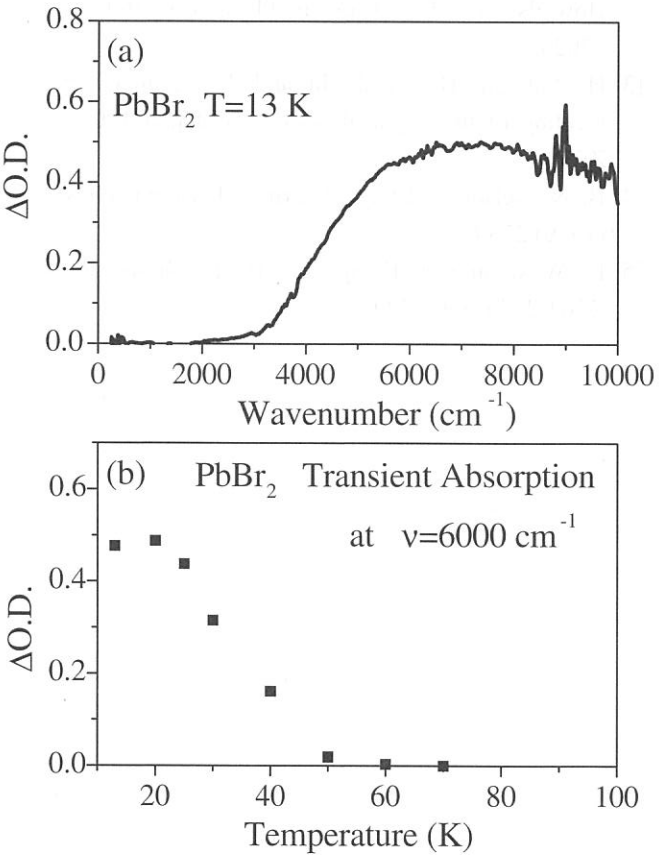

Fig.1 (a): Transient absorption spectrum in lead bromide at 13 K. (b): Temperature dependence of the transient absorption at 6000 cm^{-1}.

suggested that the free electron-hole pair is relaxed into the spatially separated pair of a self-trapped electron and a self-trapped hole by the strong electron-lattice interaction[4,5]. This is an interesting suggestion which pushes us to study the relaxation process of the photo-excited states.

Figure 1(a) shows the transient absorption spectra of lead bromide at 13 K. One can see that a broad transient absorption band appears above 3000 cm^{-1}. This absorption band disappeared instantly after the laser excitation was stopped. This indicates that the absorption is not due to the sample damage caused by the laser irradiation.

Figure 1(b) shows the temperature dependence of the transient absorption at 6000 cm^{-1}. It is clear that the transient absorption decreases around 40 K. The electron-spin-resonance measurement performed by Iwanaga *et al.* has clarified that the V_k-type hole center (Br_2^- dimer center) is induced as a self-trapped hole by the photo-excitation and disappears above 40 K[6]. This result indicates that the observed transient absorption is due to the self-trapped hole. The present experiment is the first optical observation about the self-trapped hole in lead halides.

It is important to investigate the time evolution of the transient absorption originating from the self-trapped hole in order to clarify the relaxation dynamics of the photo-excited state in lead halides. Therefore we are planning to apply the time-resolved technique to this transient absorption measurement.

References

[1] T. Kobayashi, T. Saito and H. Ohtani, Nature **414**, 531 (2001).

[2] S. Iwai, S. Tanaka, K. Fujinuma, H. Kishida, H. Okamoto and Y. Tokura, Phys. Rev. Lett. **88**, 057402 (2002).

[3] M. Nagai, R Shimano and M. Kuwata-Gonokami, Phys. Rev. Lett. **86**, 5759 (2001).

[4] M. Iwanaga, M. Watanabe and T. Hayashi, Phys. Rev. B **62**, 10766 (2000).

[5] M. Kitaura and H. Nakagawa, J. Phys. Soc. Jpn. **70,** 2462 (2001).

[6] M. Iwanaga, J. Azuma, M. Shirai, K. Tanaka and T. Hayashi, cond-mat/0201264.

(BL6A1&7B)

Optical response of $Cu_{1-x}Zn_xIr_2S_4$ due to metal-insulator transition

L. Chen[1], M.Matsunami[1], T.Nanba[1], G.Cao[2] and T.Matsumoto[2]

1.*Graduate School of Science and technology, Kobe University, Nada-ku, 657-8501, Kobe, Japan*

2.*National Research Institute for Metals, 1-2-1Sengen, Tsukuba, 305-0047, Japan*

The mother material $CuIr_2S_4$ of the thiospinel system $Cu_{1-x}Zn_xIr_2S_4$ undergoes a temperature-induced metal-insulator (M-I) transition around 226 K and its precise change in the optical conductivity spectrum due to MI transition has been reported. [1] The Zn substitution for Cu suppresses the MI transition temperature (T_{MI}), resulting in the complete suppression of the MI transition for $x > 0.4$ and also appearance of superconductivity for $x>0.25$ [2]. From the measurements of magnetic susceptibility, X-ray diffraction, and photoelectron spectroscopy, the appearance of the insulating state is to be explained in terms of charge ordering of the Ir3+ and Ir^{4+} ions due to the Ir^{4+} dimerization coupled with the slight deformation of the S-octahedron surrounding the Ir ion. From the band calculation [2], it has been pointed out that the hybridization band across the Fermi level (E_F) formed by the Ir-5d (t_{2g}) and S-3p states play an important role in its material properties. However, the precise study of the change in the electronic structure has not been done on the M-I transition. We have measured the temperature dependence of the optical reflection spectra of $Cu1_{-x}Zn_xIr_2S_4$ (x=0, 0.1, 0.3, 0.4 and 0.5) samples in the energy regions of 0.005-30 eV in order to study the change in the electronic structure very close to the E_F due to the Zn substitution for Cu. Measured reflection spectrum of $Cu_{1-x}Zn_xIr_2S_4$ **in** the temperatures of 8-300 K and its optical conductivity spectrum, $\sigma(\omega)$, obtained by a Kramers-Kronig transformation of the reflection spectrum are shown in Fig.1 for x=0.1. In metallic state above $T_{MI} \sim 130$ K, the Drude part was found to be composed of two components which correspond to the two branches around Γ at B.Z across the E_F in the energy band calculation. Each branch gives rise to a different Drude component because of the difference in the effective mass and lifetime. The continuous Drude components in metallic state lose its intensities below T_{MI} and the interband peak appeared in insulating state in the lower energy part of the spectrum although the higher energy part ($h\nu \geq 3eV$) does not almost change. Only slight change in the whole spectrum except the the lower energy part means that the change in material properties like a MI transition is induced by the change in the electronic state very close to E_F.

The lowest energy interband peak (L) at 0.5 eV for x=0 split into two peaks L_1 and L_2 for x=0.1 and 0.3. The intensities of these peaks do not increase with increasing of Zn substitution as shown in Fig.2. This means that the electronic states very close to the E_F does not come from Zn but the degree of the hybridization between the Ir-5d(t_{2g}) and S-3p states is affected by the Zn substitution.

References

[1] M.Hayashi et al.:Physica **B** 281&282(2000)631.

[2] T.Furubayashi *et al.*: J.Phys.Soc.Lapan **63**(1994)3333.

[3] T.Oda. *et al.* : J.Phys.:Condens.Matter **7**(1995)4433.

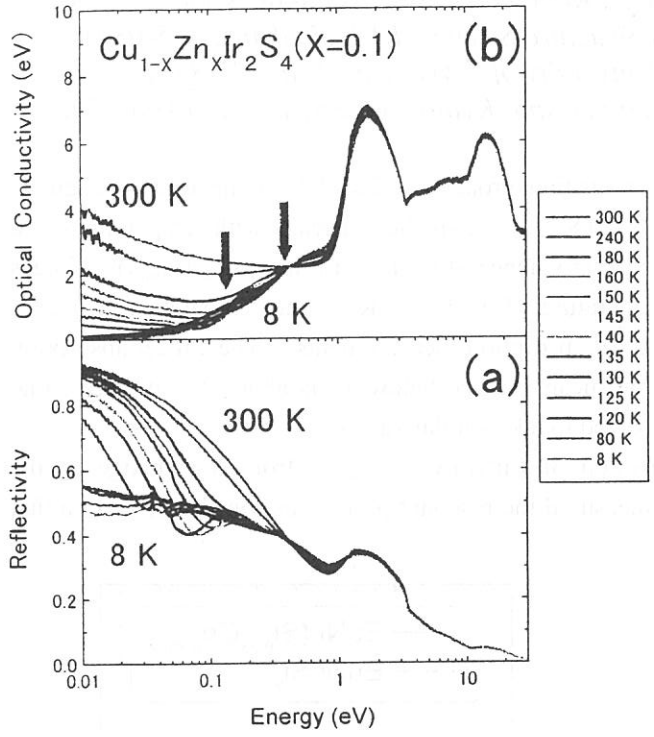

Fig.1

Measured reflection (b) $Cu_{0.9}Zn_{0.1}Ir_2S_4$ and its optical conductivity spectra, σ(a).

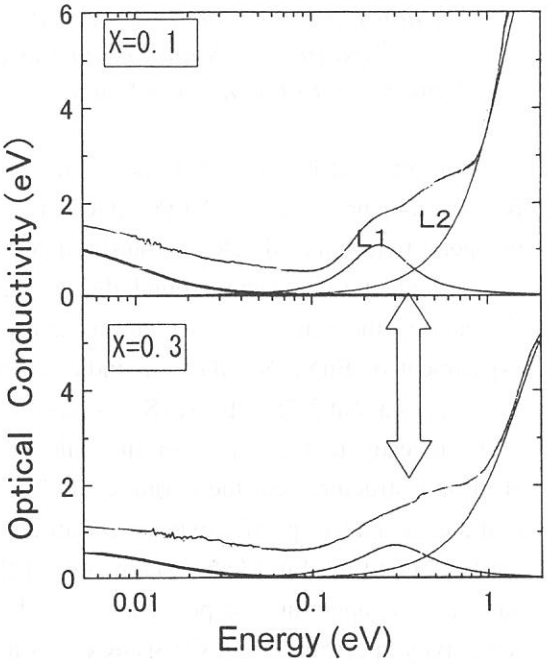

Fig.2 Splitting of the lowest energy interband peak (L) around 0.4 eV for x=0 to the peaks L_1 and L_2 for x=0.1 and 0.3, and its dependence on Zn substitution.

(BL6A1)

Temperature-Induced Valence Transition of $EuNi_2(Si_{0.25}Ge_{0.75})_2$ Studied by Eu 4*d*-4*f* Resonant Photoemission and Optical Conductivity

S. Kimura[1], M. Okuno[1], H. Iwata[1], T. Saitoh[2], T. Okuda[3], A. Harasawa[3], T. Kinoshita[3], A. Mitsuda[3], H. Wada[4] and M. Shiga[4]

[1]*Graduate School of Science and Technology, Kobe University, Nada-ku, Kobe 657-8501*
[2]*Photon Factory, Institute of Materials Structure Science, KEK, Tsukuba, 305-0801*
[3]*Institute for Solid State Physics, University of Tokyo, Kashiwa, 277-8581*
[4]*Dapartment of Materials Science and Engineering, Kyoto University, Kyoto 606-8501*

Some rare-earth compounds have the valence transition property induced by temperature, magnetic fields and/or pressure. $EuNi_2(Si_{1-x}Ge_x)_2$ (x = 0.70 - 0.82) is one of the materials with temperature- and magnetic field-induced valence transition.[1] The mean valence of Eu ion in $EuNi_2(Si_{0.25}Ge_{0.75})_2$ changes from trivalent to divalent around the critical temperature (T_V) of 115 K as the temperature increases detected by the magnetic susceptibility and the Eu 2*p* absorption measurements. The Eu 2*p* absorption experiment of $EuNi_2(Si_{0.21}Ge_{0.79})_2$ indicated that the mean valence below T_V is about 2.8, whereas, that above T_V is about 2.25. $EuNi_2(Si_{0.25}Ge_{0.75})_2$ is expected to take similar valences.

To investigate the origin of the valence transition of $EuNi_2(Si_{0.25}Ge_{0.75})_2$ from the change of the electronic structure near the Fermi level (E_F), we measured the resonant photoemission (RPE) spectra that is the elementally specific experiment around the Eu 4*d* and the Eu 3*d* absorption edges [2] and the temperature dependence of the reflectivity spectrum of $EuNi_2(Si_{0.25}Ge_{0.75})_2$ in the infrared - vacuum-ultraviolet range [3]. The material with trivalent Eu ion, $EuNi_2Si_2$, was also examined for the reference. The optical conductivity ($\sigma(\omega)$) spectra are compared to the RPE spectra and the change of the electronic structure due to the valence transition is discussed.

The Eu 4*d*-4*f* RPE experiment was performed at the beam line 11D of Photon Factory, where a high energy-resolution electron spectrometer, SCIENTA SES-200, is equipped. The total resolution of the monochromator and the electron analyzer was estimated to be about 50 meV at $h\nu \sim$ 140 eV. The sample was set several temperatures of 15 – 300 K controlled by continuous flow of liquid helium and a heater. Samples was scraped *in situ* by a diamond file under ultra-high vacuum. The infrared reflectivity spectra were recorded at the beam line 6A1of UVSOR.

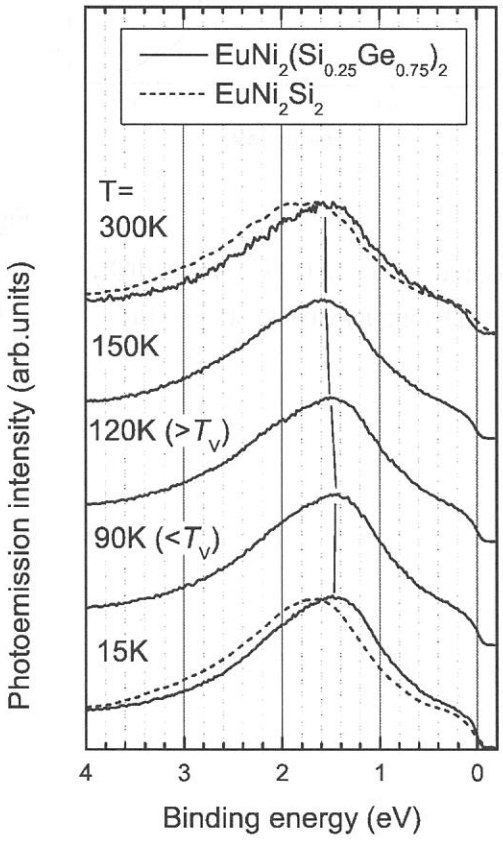

Fig. 1. Temperature dependence of off-resonant photoemission spectrum of $EuNi_2(Si_{0.25}Ge_{0.75})_2$ (solid lines) at $h\nu$ = 135.9 eV. The spectra of $EuNi_2Si_2$ at 15 and 300 K are also plotted for the reference (dotted lines).

The change of the other electronic structure due to the valence transition is examined by using the off-RPE spectra. Figure 1 is the temperature dependence of the off-RPE spectrum of $EuNi_2(Si_{0.25}Ge_{0.75})_2$ at $h\nu$ = 135.9 eV. The spectra of $EuNi_2Si_2$ at 15 and 300 K are also plotted. The spectra mainly correspond to the Ni 3*d* partial density of states. In $EuNi_2Si_2$, the peak is located at higher binding energy (E_B) side than that of $EuNi_2(Si_{0.25}Ge_{0.75})_2$. The peak of $EuNi_2Si_2$ expands with increasing temperature but the peak energy does not shift. On the other hand, the peak of $EuNi_2(Si_{0.25}Ge_{0.75})_2$ that is located at 1.5 eV below T_V slightly shifts to the high E_B by 0.1 eV above T_V. This indicates that the valence of Ni slightly decreases above T_V. At the Eu site, Eu^{2+} is dominant above T_V. Therefore both mean valences of Eu and Ni decrease above T_V. The reason is that the mixing between Eu^{3+} 4*f*-hole and Ni 3*d* becomes weak above T_V because the Eu^{3+} state decreases.

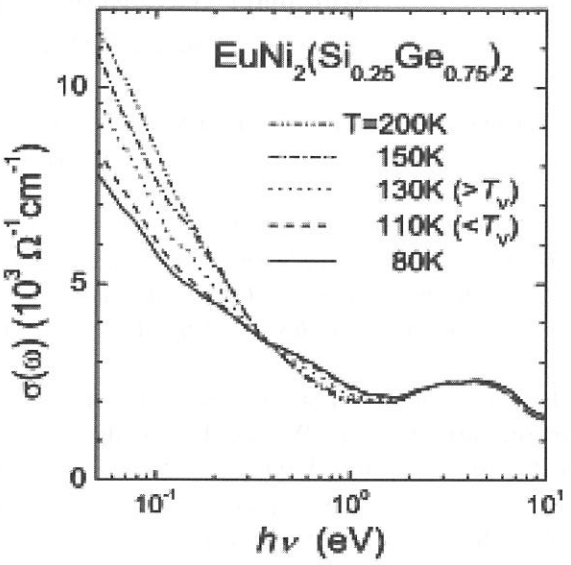

Fig. 2. Temperature dependence of optical conductivity spectrum ($\sigma(\omega)$) of $EuNi_2(Si_{0.25}Ge_{0.75})_2$.

The character of carriers is considered. Since the 4f state has no density at the E_F of E_B = 0 and the Ni 3*d* state has the density at the E_F, the conduction band originate from the Ni 3*d* state. The density of the Ni 3*d* state on the E_F decreases as the temperature increases despite that of $EuNi_2Si_2$ does not change with the temperature. The change appears in the $\sigma(\omega)$ spectrum in Figure 2. The $\sigma(\omega)$ spectrum below 2 eV that has a gentle slope to the low energy side below T_V gradually changes to the steep slope above T_V. The change is different from that of a normal metal, *i.e.*, the slope becomes gentle as the temperature increases because the relaxation time becomes long in a normal metal. The short (long) relaxation time means that the mixing intensity between the Ni 3*d* conduction band and the Eu^{3+} 4*f*-hole states is strong (weak). Therefore the mixing intensity below T_V is larger than that above T_V. This is consistent with the valence transition from trivalent to divalent with increasing temperature.

The photon energy at which the $\sigma(\omega)$ spectrum becomes minimum corresponds to the plasma frequency of carriers. The square of the photon energy is proportional to the carrier density. Since the photon energy of the minimum $\sigma(\omega)$ shifts to the low energy side with increasing temperature, the carrier density below T_V is higher than that above T_V. This result is consistent with the temperature dependence of the Ni 3*d* states on the E_F observed in Fig. 1. Therefore the carrier mainly originates from the Ni 3*d* states.

Reference

[1] H. Wada *et al.*, J. Phys., Condens. Matter **9** (1997) 7913.

[2] T. Kinoshita *et al.*, J. Phys. Soc. Jpn. **71** (2002) 148.

[3] S. Kimura *et al.*, J. Phys. Soc. Jpn.**71** (2002) in press.

(BL6A1)

Millimeter Wave Reflection Measurements of $LiNiO_2$ Using UVSOR and Coherent SR

Hitoshi Ohta, Kanji Kawakami[A], Yuta Nagasaka[A], Takao Nanba[A], Atushi Hirano[B], Ryoji Kanno[B], T. Takahashi[C] and T. Matsuyama[C]

Molecular Photoscience Research Center, Kobe University, 1-1 Rokkodai, Nada, Kobe 657-8501
[A]The Graduate School of Science and Technology, Kobe University, 1-1 Rokkodai, Nada, Kobe 657-8501
[B]Department of Chemistry, Faculty of Science, Kobe University, 1-1 Rokkodai, Nada, Kobe 657-8501
[C]Research Reactor Institute Kyoto University, 1010 Noda, Kumatori, Sennan, Osaka 590-0494

$LiNiO_2$ is known as a super ionic conductor and also a promising material for the positive electrode of the Li ion secondary batteries. We have been studying the millimeter wave reflection measurements of $LiNiO_2$ and related substances using UVSOR [1-6]. We found the drastic increase of the reflection of $LiNiO_2$ above 300 K in the millimeter wave region [1, 6], and we suggested that this increase of reflection is related to the motion of Li ion in the system. However, it is difficult to extend our measurement below 5 cm^{-1} in UVSOR. As the coherent SR of Kyoto University in Kumatori has a potensial to extend our study, we started a measurement using coherent SR and compared it with the result using UVSOR.

The reflection measurements of $LiNiO_2$ sintered sample with a diameter of 10 mm have been performed in the spectra region from 5 to 60 cm^{-1} and 5 to 18 cm^{-1} using the beam line BL6A1 of UVSOR and the coherent SR produced by the LINAC of Kyoto University in Kumatori, respectively. The measurement using coherent SR was limited down to 5 cm^{-1} due to the sample diameter. The temperature was changed from 300 to 380 K. The gold plate was used as a reference and InSb detector was used as a detector. Figure 1 shows our results for $LiNiO_2$ sample. The results of UVSOR and coherent SR observed at 300, 340 and 380 K are consistent within the limit of the S/N ratio. From these results we can extend our study below 5 cm^{-1} using the larger diameter sample and discuss about the origin of the reflection in high temperature.

[1] H. Ohta *et al.*: UVSOR Activity Report 1996 (1997) 182.
[2] H. Ohta *et al.*: UVSOR Activity Report 1997 (1998) 128.
[3] H. Ohta *et al.*: UVSOR Activity Report 1998 (1999) 158.
[4] H. Ohta *et al.*: UVSOR Activity Report 1999 (2000) 93.
[5]H. Ohta *et al.*: UVSOR Activity Report 2000, (2001) 121.
[6] H. Ohta *et al.*: Jpn. J. Applied Phys. **39** (2000) Suppl. 39-1, 409-410.

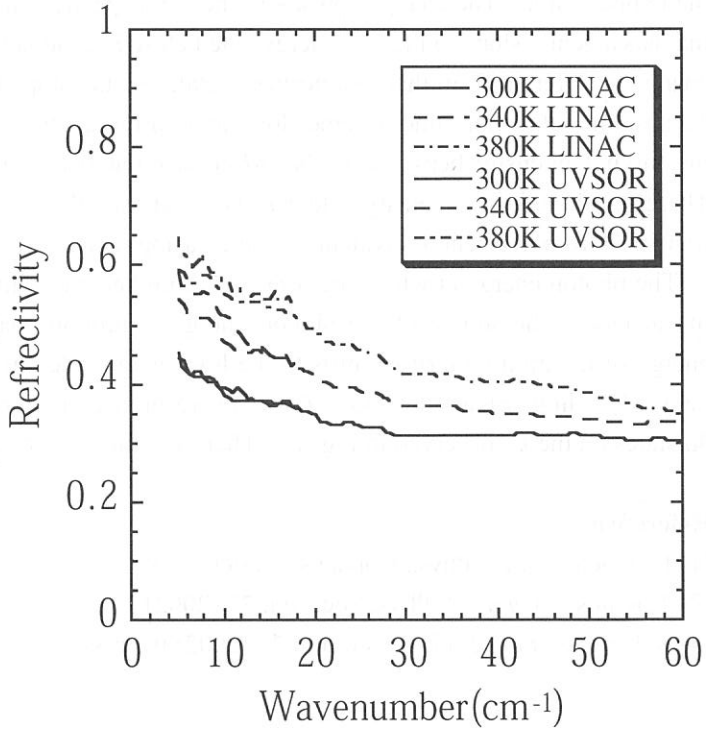

Fig. 1 Reflection spectra of $LiNiO_2$.

(BL7B)

Excitonic properties of lead-halogen-based self-organized low-dimensional crystals

Kenichiro Tanaka[a, b], Takayuki Takahashi[a, b], Takashi Kondo[a, b]

[a]*Department of Materials Science, The University of Tokyo, 7-3-1 Hongo, Bunkyo-ku, Tokyo 113-8656, Japan*

[b]*Core Research for Evolutional Science and Technology, Japan Science and Technology Corporation (CREST)*

The large family of the lead-halogen-based perovskite-type crystals have been attracted much attention because of their unique crystal structures and the optical properties. They are self-organized low-dimensional crystals, where $[PbI_6]$ octahedra form zero-, one-, two- or three-dimensional networks. In these crystals, excitonic absorption peaks are clearly observable, mainly because they are tightly confined in the $[PbI_6]$ networks. In the past study, it has shown that the excitonic effects are strengthened according as the dimensionality of the $[PbI_6]$ octahedra networks are lowered. Further investigation of the excitonic properties of these materials needs the clarification of the electronic structure of these materials. Thus we measured the reflectivity spectra in this study on $(C_6H_{13}NH_3)_2PbI_4$ (two-dimensional crystal), $(CH_3NH_3)PbBr_3$ (three-dimensional crystal), and $[NH_2SC(=NH_2)NH_2]_3PbI_5$ (one-dimensional crystal) at 18 K. The light was focused onto the sample with nearly normal incidents and the reflected light was detected by Si photodiode. Figure shows the absorption spectra of $(C_6H_{13}NH_3)_2PbI_4$, $(CH_3NH_3)PbBr_3$ and $[NH_2SC(=NH_2)NH_2]_3PbI_5$ evaluated from the Kramers-Kronig transformation of the reflectivity spectra obtained in this study. In each crystal, the clear exciton absorption lines were clearly observed. The oscillator strength of the lowest-energy exciton $(C_6H_{13}NH_3)_2PbI_4$, $[NH_2SC(=NH_2)NH_2]_3PbI_5$ and $(CH_3NH_3)PbBr_3$ are evaluated to be 0.8, 0.5 and 0.03 per $[PbI_6]$ octahedron unit, respectively. The excitons confined in lower structures such as $(C_6H_{13}NH_3)_2PbI_4$ and $[NH_2SC(=NH_2)NH_2]_3PbI_5$ have much higher oscillator strength than the three dimensional crystal $(CH_3NH_3)PbBr_3$. The origins of the absorption band appeared above the lowest-energy excitons are under investigation by several measurements such as two-photon absorption and electroabsorption spectroscopy.

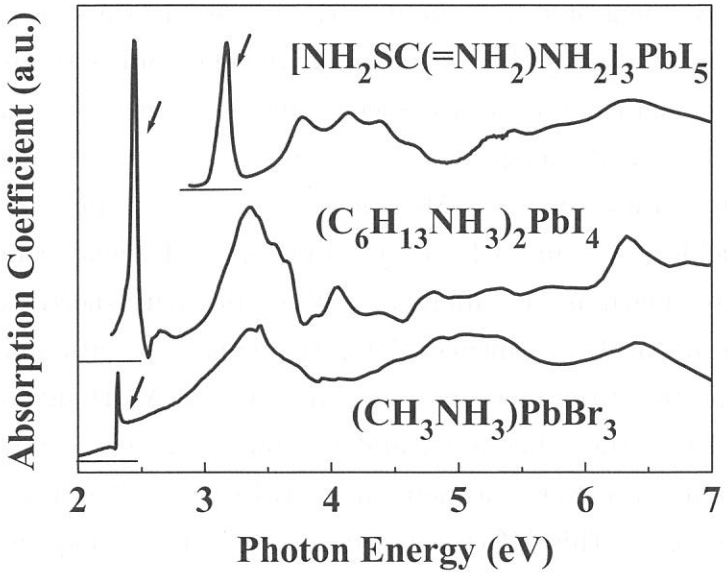

Fig. The absorption spectra of $[NH_2SC(NH_2)NH_2]_3PbI_5$, $(C_6H_{13}NH_3)_2PbI_4$ and $(CH_3NH_3)PbBr_3$ at 18 K. The arrows show the lowest-energy exciton.

(BL6A1)

Infrared magnetic circular dichroism in the colossal magneto- resistance pyrochlore $Tl_2Mn_2O_7$

H. Okamura, T. Koretsune, M. Matsunami, S. Kimura, T. Nanba,
H. Imai[A], Y. Shimakawa[A], Y. Kubo[A]

Department of Physics and Graduate School of Science and Technology, Kobe University, Kobe 657-8501.
[A]Fundamental Research Laboratories, NEC Corporation, Tsukuba 305-8501, JAPAN

Physics of the colossal magneto-resistance (CMR) phenomena has been one of the central issues of condensed matter physics in the last several years. In particular, the ferromagnetic perovskite manganites, e.g., $La_{1-x}Sr_xMnO_3$, have attracted much attention [1]. More recently, the $Tl_2Mn_2O_7$ pyrochlore has been attaining increasing interest, since it exhibits a CMR that is comparable to those observed for the perovskites [2]. $Tl_2Mn_2O_7$ is also a ferromagnet, and its resistivity (ρ) drops rapidly upon cooling through $T_c \sim 120$ K. Near and above T_c, an external magnetic field of 7 T reduces ρ by a factor of ~ 10. Although these features appear very similar to those for the perovskites, various studies have suggested that the underlying mechanism should be very different from that in the perovskites [2]. In order to study the electronic structures of $Tl_2Mn_2O_7$, we have measured its optical reflectivity spectra under magnetic fields at BL6A1 [3], and observed an infrared (IR) magnetic circular dichroism (MCD). Figure shows the reflectivity spectra (top graphs) and the MCD spectra (bottom graphs) of $Tl_2Mn_2O_7$ at 40 K under magnetic fields of 4 T and 6 T measured under the Faraday configuration. Here, the MCD spectra are shown as the difference of the reflectivity spectra when the field direction is changed from parallel to antiparallel to the light propagation direction, normalized by the average spectra of the two configurations. A clear MCD signal is observed exactly at the plasma edge of the reflectivity, and it grows with increasing magnetic field. Using this MCD signal, the Kerr rotation can be calculated. The rotation angle is of the order of a few degrees. This MCD signal decreases with increasing temperature, and it becomes very weak above ~140 K. In addition, the MCD grows with magnetic field even at 40 K, where the magnetization is almost saturated below 0.5 T. Our analyses have shown that a simple magneto-plasma model is able to account for the basic features of this MCD signal. In this model, an MCD arises from the coupled Drude-cyclotron motion of a plasma, and a ferromagnetic spin order is not required to produce an MCD. For an MCD in a

ferromagnetic material, the magnitude of the observed MCD signal is known to be proportional to the spontaneous magnetization, and also the MCD is a result of a spin-orbit coupling that connects the spin state of the electrons with the circular polarization of light. The observations that the observed MCD is not proportional to the magnetization and that the MCD is basically reproduced by a classical magneto-plasma suggest that the spin-orbit coupling is rather weak in this compound. Further analyses are in progress for a better understanding of this compound.

References

[1] See, for example, Y. Tokura et al. J. Phys. Soc. Jpn. **63**, 3931 (1994).

[2] Y. Shimakawa et al., Nature **379**, 53 (1996); Phys. Rev. B **55**, 6399 (1997).

[3] H. Okamura et al., Phys. Rev. B 64, 180409(R) (2001).

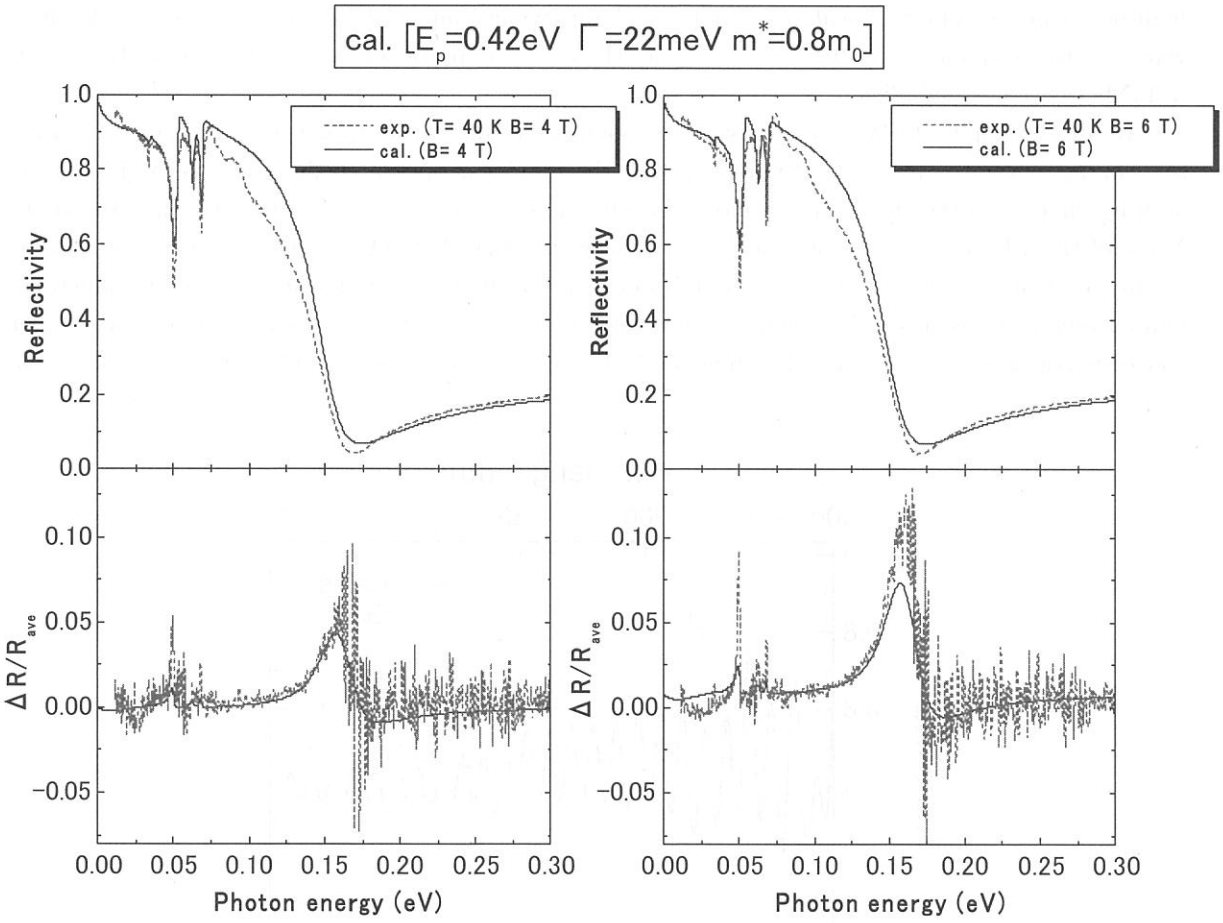

FIGURE: Top graphs: optical reflectivity spectra of $Tl_2Mn_2O_7$ at 40 K, under magnetic fields of 4 T and 6 T. Bottom graphs: the MCD spectra, given as the difference of reflectivity spectra when the magnetic field direction is flipped.

(BL6A1)

Transmittance spectra of GaAs and GaP in far-infrared region

Ichiro Shoji and Takunori Taira

Laser Research Center for Molecular Science, Institute for Molecular Science, 38 Nishigonaka, Myodaiji, Okazaki 444-8585, Japan

Demands for wide-tunable infrared (IR) coherent light sources are growing because they can be used for a variety of applications, including spectroscopy, chemical monitoring, biomedical applications, and atmospheric and environmental sensing. Frequency down conversion of 1 μm pump sources such as Nd:YAG lasers which uses optical parametric oscillation or difference-frequency generation is a promising approach to obtain coherent light in the IR region. It is necessary to satisfy the phase-matching condition between the pump, signal, and idler light in order to realize high conversion efficiency. The conventional phase-matching method using birefringence in nonlinear-optical crystals limits the wavelength range and materials applicable, while quasi-phase matching (QPM) technique which periodically modulates the magnitude of the nonlinear-optical coefficient has many advantages and has been intensively studied. Especially, recent developments in fabrication of periodically poled $LiNbO_3$ (PPLN) [1] have realized high-power pulse and cw optical parametric oscillators which emit up to 4 μm. However, highly efficient wavelength conversion using PPLN is difficult for the wavelengths longer than 6 μm because IR absorption in $LiNbO_3$ becomes significant.

We are developing QPM devices using compound semiconductors to generate IR light. Compound semiconductors have large optical nonlinearities; the nonlinear optical coefficient of GaAs is 170 pm/V at wavelength of 1.06 μm, which is more than 6 times larger than that of $LiNbO_3$ [2]. In addition, Many of them have longer absorption cutoff wavelengths than $LiNbO_3$; GaAs is transparent as long as 16 μm [3]. Moreover, the crystal-growth and processing technologies are matured for semiconductors [4]. Our current target is developing highly efficient mid-IR sources, but it would be attractive if the frequency conversion devices generating far-IR can be made by use of compound semiconductors. We have measured

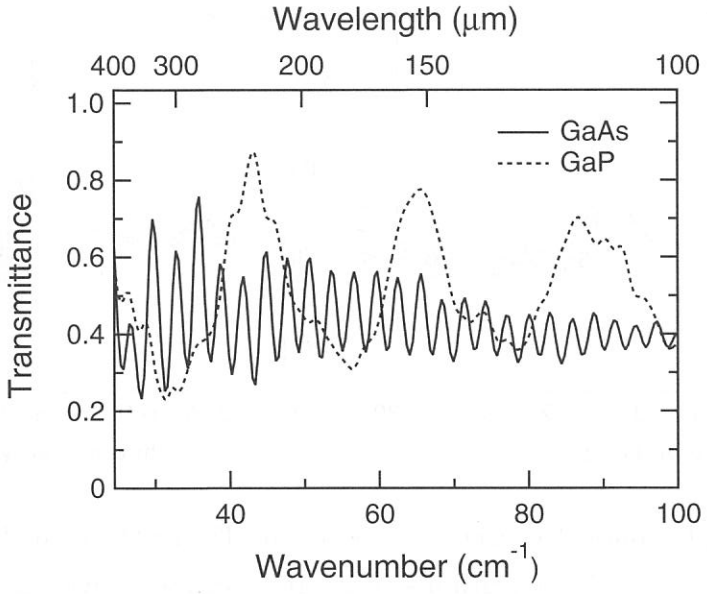

Fig 1. Transmittance spectra of the undoped GaAs and GaP in far-IR region.

transmittance spectra of GaAs and GaP, which are popular compound semiconductors, in far-IR region to investigate the possibility for far-IR generating materials.

Absorption spectra of semiconductors strongly depend on the dopant concentration. Semi-insulating or high-resistivity samples are suitable for frequency-conversion devices because the optical absorption is much lower. We have prepared an undoped GaAs and GaP samples grown by Hitachi Cable and Sumitomo electric, respectively. The resistivities were both $\geq 10^7\ \Omega\,\mathrm{cm}$, the thicknesses were 470 and 75 μm, respectively, and their both facets were optically polished. The absorption spectra were measured with the Martin-Puplett Fourier interferometer (Specac) at the beam line BL6A1. Using the Si bolometer, we made measurements in the wavelength range of 100–400 μm (25–100 cm^{-1}). The step and the total displacement of the moving mirror were 25 μm and 6.4 mm, respectively.

Figure 1 shows the obtained transmittance spectra. We found that both GaAs and GaP are transparent in the measured region, although transmittances are lower than in the near-IR region because the refractive indices in far-IR are much higher. The modulations in the obtained spectra are due to the interference effects caused by the multiple reflections of the beam since the samples were plane-parallel plates.

We have found that GaAs and GaP are attractive materials for the frequency conversion devices generating far-IR light.

References

[1] L. E. Myers, R. C. Eckardt, M. M. Fejer, R. L. Byer, W. R. Bosenberg, and J. W. Pierce, J. Opt. Soc. Am. B **12,** 2102 (1995).

[2] I. Shoji, T. Kondo, A. Kitamoto, M. Shirane, and R. Ito, J. Opt. Soc. Am. B **14,** 2268 – 2294 (1997).

[3] I. Shoji, S. Kurimura, and T. Taira, "Infrared absorption spectrum of GaAs," UVSOR ACTIVITY REPORT 2000.

[4] S. Koh, T. Kondo, M. Ebihara, T. Ishiwada, H. Sawada, H. Ichinose, I. Shoji, and R. Ito, "GaAs/Ge/GaAs sublattice reversal epitaxy on GaAs (100) and (111) substrate for nonlinear optical devices," Jpn. J. Appl. Phys. **38,** L508 – L511 (1999).

(BL7A)

In situ measurement of luminescence from silica glass under soft X-ray irradiation

Tomoko Yoshida[A], Tetsuo Tanabe[A], Hisao Yoshida[B]

[A]*Center for Integrated Research in Science and Engineering, Nagoya University, Nagoya 464-8603, Japan*

[B]*Department of Nuclear Engineering, Graduate School of Engineering, Nagoya University, Nagoya 464-8603, Japan*

Introduction

Radiation effects on silica glasses are one of the main concerns for their application as optical windows, insulators and optical fibers under fusion and fission environments.[1] Although the radiation damage of silica in nuclear environments has been widely studied, the detailed damaging process and damage structure are still unknown. That is mainly because the effect of ionizing radiation, which is very important in optical materials like silica, is mixed up with the displacement effect. Recently, we have made in-situ luminescence measurements of silica glasses induced by in-reactor irradiation. This in-situ measurement was very useful for the observation of dynamic effects of ionizing radiation on the electrical property of a silica [2,3] and we have applied this technique to study effects of other ionizing radiations (such as gamma-ray, X-ray VUV and UV lights) on silica.

The present work is our first trial to observe soft X-ray radiation effects on silica. We have measured the luminescence from a silica glass under the irradiation of soft X-ray near Si K-edge, and investigated the origin of the luminescence.

Experimental

The samples used in this work was a fused silica glass (T-1030) of 13 mm diameter and 2 mm thickness produced by Toshiba Ceramics, Japan. The measurement of luminescence of a fused silica glass induced by soft X-ray irradiation (1.8-1.9 keV) was carried out on the beam line 7A at UVSOR, Institute for Molecular Science with a stored current of 100-200 mA. The luminescence was focused by a lens in the UHV chamber to the monochromator (CP-200, JOBIN YVON) and detected by a multi-channel analyser (OMA III, EG&G PRINCETON APPLIED RESEARCH). The wavelength range (λ) from 300 to 800 nm was measured because the photon detecting efficiency in the regions of $\lambda <$ 300 nm and $\lambda >$ 800 nm were reduced drastically. The luminescence yield spectrum was also measured by a photomultiplier (Hamamatsu Photonics R955).

Results and Discussion

Fig. 1 shows the observed luminescence spectra of the fused silica glass under the irradiation of soft X-rays near Si K-edge (1848 eV). An intense emission band at around 400 nm was observed. Similar luminescence spectra have been measured for silica glasses under in-reactor or UV irradiation [2,3], and we have concluded that the present XEOL, 400 nm band emission, originates from an intrinsic $B_{2\beta}$ center [4] due to the electron excitation by soft X-ray.

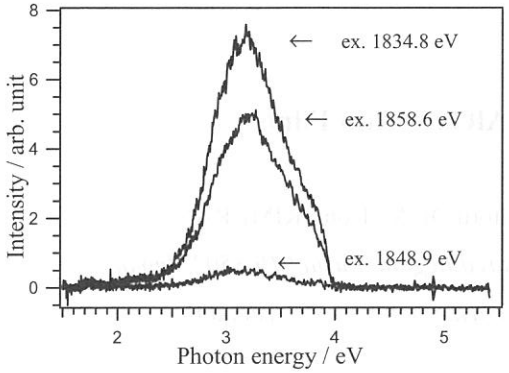

Fig.1 Optical luminescence spectra of a fused silica glass excited by soft X-ray with the energy of 1834.8 eV, 1848.9 eV and 1858.6 eV.

It is noteworthy that the intensity of the 400 nm emission band changed with the excitation energy of soft X-ray (Fig.1). Therefore, we also measured a photoluminescence yield (PLY) spectrum of the 400 nm band and showed in Fig. 2(a) together with X-ray absorption (Si K-edge XANES) spectrum (Fig. 2(b)) recorded in the photocurrent mode for the same fused silica glass. It is rather surprising to see nice correspondence between the PLY and XANES spectra. Three processes are controlling the photoluminescence yield. One is penetration depth or energy deposition per unit volume of the incident soft X-ray. But one should note that only very small fraction of the deposited energy is used for activation or electron excitation of the $B_{2\beta}$ center. Nevertheless, two following processes can be distinguished. One is electron excitation density and the other is relaxation probability of the excited electrons through the $B_{2\beta}$ emission. However, in the present stage, none of above three processes are evaluated quantitatively and further studies are necessary.

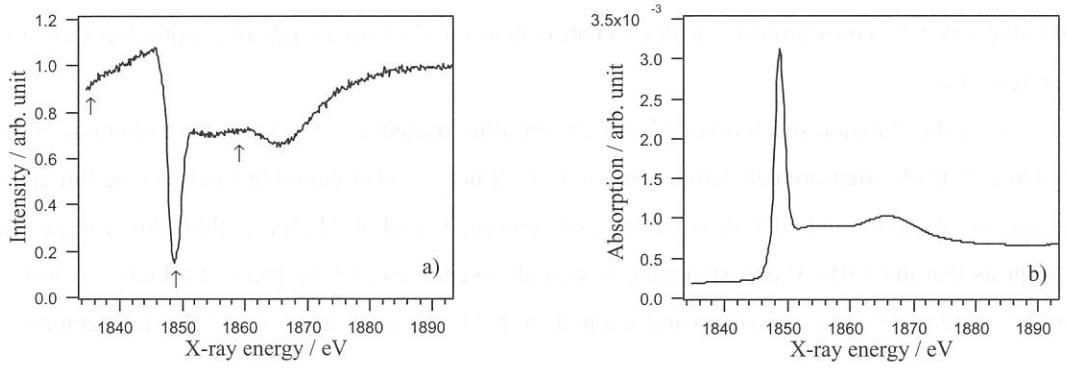

Fig. 2 The comparison between a) the luminescence yield spectrum of the 400 nm band and b) Si K-edge XANES spectrum of a fused silica glass.

Acknowledgements

The authors are grateful to Prof. Eiji Sigemasa, Prof. Masao Kamata and Mr. Eiken Nakamura of UVSOR for their great help and cooperation in the luminescence measurements.

References

[1] F.W. Clinard Jr., L.W. Hobbs, in: Physics of Radiation Effects in Crystal, Elsevier, Amsterdam, 1986, p. 442.

[2] T. Yoshida, T. Tanabe, T. Ii, T. Hara, M. Sakai and Y. Inaki, *Nucl. Instr. and Meth. B*, 166-167 (2000) 476.

[3] T. Ii, T. Yoshida, T. Tanabe, T. Hara, M. Okada and K. Yamaguchi, *J. Nucl. Mater.* 283-287 (2000) 898.

[4] R. Tohmon, H. Mizuno, Y. Ohki, K. Sasagane, K. Nagasawa, Y. Hama, *Phys. Rev. B* 55 (1989) 1337.

(BL7B)

Luminescence Spectra of AlGaN Thin Films

Kazutoshi FUKUI, Kazuya EBISU[1], Satoru ODA[1], Kouji KIMURA[1]

Research Center for Development of Far-Infrared Region, Fukui 910-8507, Japan

[1] Faculty of Engineering, Fukui University, Fukui 910-8507, Japan

The group III-nitride semiconductors (AlN, GaN and InN) are promising materials for applicateions in opt-electronic devices. The ternary alloy $Al_{1-x}Ga_xN$ is complete solid solution and varies its band gap from 3.4 eV (blue) to 6.2 eV (ultraviolet). We have been performed the reflectance measurements at the visible – vacuum ultraviolet region [1]. In this report, we represent the emission and excitation spectra, and decay profiles.

AlGaN samples were made by MOCVD method at RIKEN on SiC substrates. The luminescence experiments were carried out as follows; a) excitation : BL7B (3.4 – 25 eV) b) luminescence : VIS – UV monoochromator (1.5 – 6.2 eV) with a CCD array c) vacuum : in the range of 10^{-9} Torr d) temperature : 17 K – 60 K e) time resolved measurement : TAC method with MCP-PMT under the single bunch operation. A single UV optical fiber cable, which was dedicated for ultra high vacuum (UHV) and had 0.6 mm core diameter, were used for detecting VIS and UV luminescence in the UHV chamber. VIS and UV luminescence lights were introduced to the VIS-UV monochromator with CCD array detector via both a UHV fiber optic feedthrough and a flexible optical fiber.

Figure 1 shows the emission spectrum of $Al_{70}Ga_{30}N$ thin film excited at 5.25 eV and the excitation spectrum that is detected at 5.05 eV. Measurement temperature is 17 K. Since no other emission bands can be found below 4.7 eV, the emission band around 5.05 eV is the only one emission band of $Al_{70}Ga_{30}N$ thin film. The excitation spectrum suggests that the 5.05 eV emission band is strongly excited around the band gap. Figure 2 shows the decay profiles of the 5.05 eV emission band excited at 5.25 eV as a function of the temperature. The

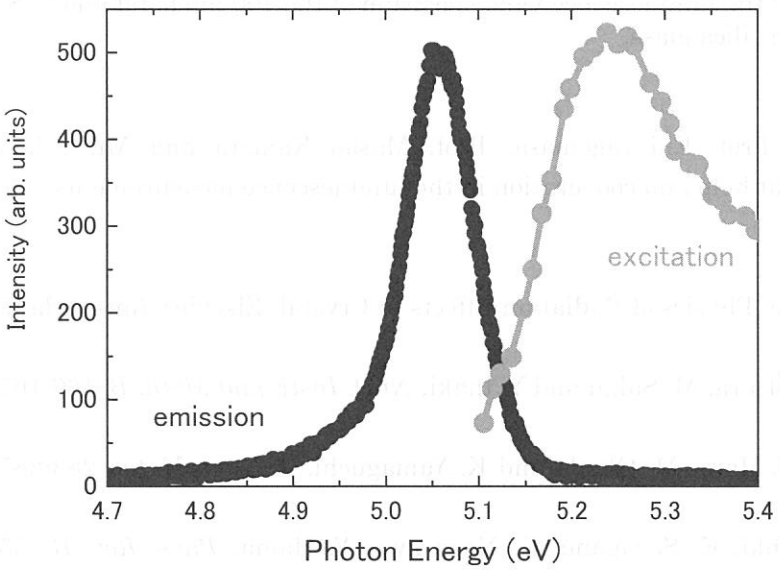

Fig.1
Excitation spectrum and emission spectrum of $Al_{0.7}Ga_{0.3}N$ at 17 K. The detected energy of the excitation spectrum and the excitation energy of the emission spectrum are 5.05 eV and 5.25 eV, respectively.

experimental results are plotted by the closed circles. Each decay profile consists of (i) sharp peak at around 0 time which is similar to the time structure of the excitation SR light (ii) non-linear decay curve in semi logarithmic graph (iii) no intensity without the noise level can observed just before 0 time. It is also clear that the overall decay time is decreasing with increasing temperature. These results suggest that there are more than three thermal activation type decay processes, one of them has the very fast decay time ($< 10^{-1}$ nsec), and the decay times of all processes are less than SR bunch period (177 nsec). The solid curves in fig. 2 are the fitting results of the combination of the two single exponential curves. Then it is concluded that there are at least three decay processes. The decay times at 17 K of $Al_{70}Ga_{30}N$ sample are $< 10^{-1}$, 0.95 and 12 nsec, for example.

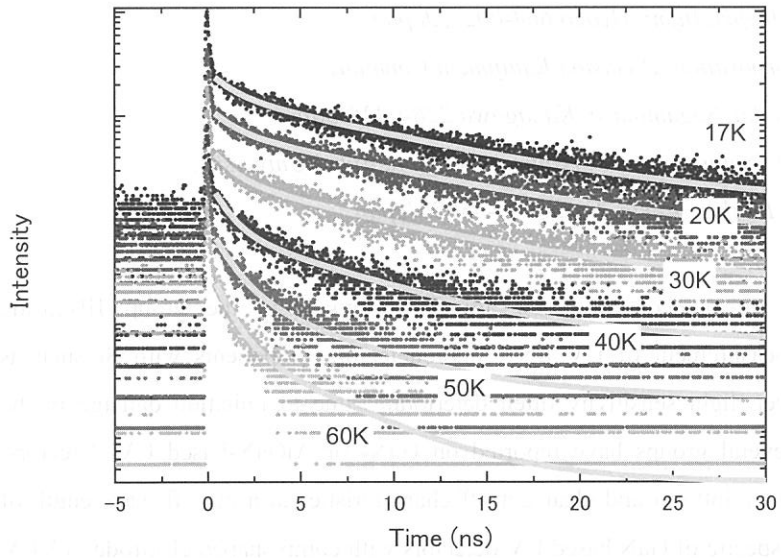

Fig.2
Decay profile of the 5.05 eV emission band excited at 5.25 eV. The measurement temperature range is from 17 K to 60 K

References

[1] K. Fukui, H. Miura, A. Okada, Q. Guo, S. Tanaka, H. Hirayama and Y. Aoyagi, Proceedings of International Workshop on Nitride Semiconductors, IPAP Conference Series 1, (2000.11) 647-650.

(BL7B)

Responsivity spectra of GaN based UV detectors in VUV region using transparent electrode

Atsushi Motogaito[1], Keiichi Ohta[1], Kazumasa Hiramatsu[1], Youichiro Ohuchi[2], Kazuyuki Tadatomo[2], Yutaka Hamamura[3] and Kazutoshi Fukui[4]

[1]*Deptartment of Electrical and Electronic Engineering, Mie University, 1515 Kamihama, Tsu, Mie 514-8507, Japan*

[2]*Telecommunication & Photonics Research Laboratory, Mitsubishi Cable Industries, Ltd., 4-3 Ikejiri, Itami, Hyogo 664-0027, Japan*

[3]*Nikon Corporation, Precision Equipment Company, 1-10-1 Asamizodai, Sagamihara, Kanagawa 228-0828, Japan*

[4]*Research Center for Development of Far-Infrared Region, Fukui University, 3-9-1 Bunkyo, Fukui, Fukui 910-8507, Japan*

Ultraviolet (UV) detectors are one of the most attractive devices in the group III-nitride semiconductors. Currently, for the measurement of UV light, photodetector components with Si such as photodiodes are mainly used. However, light sensitivity often deteriorates due to radiation damage in the vacuum ultraviolet (VUV) region. Several groups have reported on GaN- or AlGaN-based UV detectors. They have good responsivity from 250 to 360 nm and clear cut-off characteristics at a cut-off wavelength of λ_c=360 nm. We reported responsivity spectra of GaN based UV detectors with comb-shaped electrode in VUV region for the first time [1, 2]. The small responsivity in VUV region is caused by the photoemission of Au and GaN.

In this report, the responsivity spectra of UV detectors with transparent Au electrode structure to suppress the photoemission of GaN and Au are described.

The UV detectors used in this study adopt the Schottky contacts with a transparent electrode. They consist of a 3-μm-thick n-GaN layer ($n=2.0\times10^{18}$ cm^{-3}) and a 1.5-μm-thick i-GaN layer ($n=1.0\times10^{16}$ cm^{-3}) on a (0001) sapphire substrate. These layers are grown by metalorganic vapor phase epitaxy (MOVPE). The Au/Ni Schottky contact is deposited on i-GaN. The thickness of Au and Ni are 10 nm and 1 nm, respectively. The diameter of detectors is 6.5 mm.

Prior to the characterization of responsivity, the transmittance of Au in VUV region is estimated by counting the number of transmitted photons into Au membrane. Figure 1 shows transmission spectra of 10-nm-thick Au electrode. The transmittance of 10-nm-thick Au is about 0.4-0.5 in UV and VUV region and almost agreed with calculation. Thus the 10-nm-thick Au is enough thickness to transmit VUV light into Au electrode.

The responsivity spectra of detectors for photon energy are measured. Figure 2 shows the

responsivity spectra. In this measurement, the ampere meter does not measure the photoemission current of Au. Dark current is about 1-2 pA. It is corresponding to about the order of 10^{-5} A/W in Fig.2. No responsivity at the energy lower than 3.4 eV (the absorption edge of GaN) can be observed clearly. This indicates that these detectors can be used only in the UV or VUV region. The ratio of responsivity between UV and visible regions is about 5×10^{3}. The maximum responsivity of this detector is 0.15 A/W at $h\nu$=3.5 eV (λ=354 nm). The responsivity for VUV light is about 0.01 A/W. Furthermore, the photoemission current of GaN (I_{GaN}) is not detected by other measurement. It is considered that the total current measured by ampere meter is equal to diode current. Therefore, the both photoemission current of GaN and Au are not observed in this measurement and the higher responsivity is realized in this structure.

References

[1] A. Motogaito, M. Yamaguchi, K. Hiramatsu, M. Kotoh, Y. Ohuchi, K. Tadatomo, Y. Hamamura and K. Fukui: Jpn. J. Appl. Phys. **40**, L368 (2001).

[2] A. Motogaito, M. Yamaguchi, K. Hiramatsu, M. Kotoh, Y. Ohuchi, K. Tadatomo, Y. Hamamura and K. Fukui: UVSOR Activity Report 2000, 136 (2001).

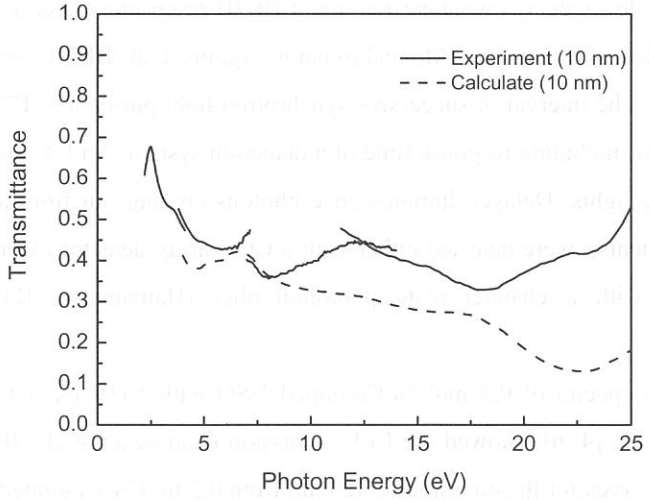

Fig.1 Transmittance spectra of 10-nm-thick Au

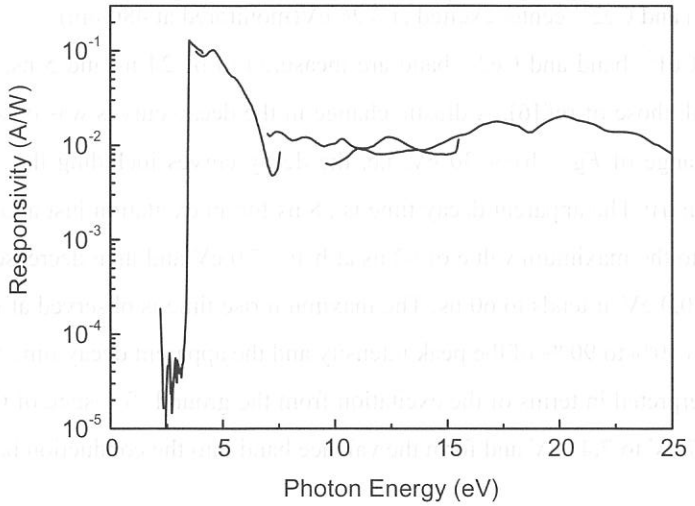

Fig.2 Responsivity spectra of UV detector with transparent Au

(BL7B)

Luminescence Decay of Ce-doped GSO under Excitation of VUV with Energy less than 30 eV at Room Temperature

S.Shimizu [a], A.Ejiri [b] and S. Kubota [a]

[a] *Rikkyo University, Nishi-Ikebukuro 3, Tokyo, 171 Japan*

[b] *Meiji University, Higashi-Sanda, Tama, Kawasaki, 214 Japan*

It is well known that the efficient scintillation photons are produced mainly through recombination of electron-hole pairs created by ionization processes with charged particles [1,2]. However, the details of the electron-hole recombination process in Ce-doped GSO (Gd_2SiO_5) have not been investigated yet, except refs.[3,4]. The purpose of this experiment is to study the energy transfer of electrons and holes to Ce^{3+} activator centers and to study the scintillation mechanism of Ce-doped GSO.

The measurements of decay curves were carried out at BL7B beam line under a single bunch operation of UVSOR. A normal incidence Mcpharson Monochromator equipped at BL7B beam line was used VUV excitation of the specimen. The interval of successive synchrotron light pulses was 177.6 ns and the duration of the pulses was about 550 ps, including response time of a detection system. An UV optical fiber cable was used for detecting luminescence lights. Delayed luminescence photons coming out from a monochromator (Model SP-300i, Princeton Instruments), were detected either with a CCD array detector (Model 1340PB) for emission spectra measurement or with a channel plate photomultiplier (Hamamatsu, R3809U) for decay curve measurement.

The observed emission spectra of 0.5 mol % Ce-doped GSO with VUV excitation at $h\nu$ higher than the band-gap energy Eg (~6.2 eV [4, 6]) showed the $Ce1^{3+}$ emission band peaking at 440 nm as reported in [5,6]. Figure 1 shows the decay curves for the emission of 420 nm from 0.5 mol % Ce-doped GSO under excitation of VUV photons between $Eg < h\nu < 30$ eV, together with the decay curves of the $Ce1^{3+}$ center excited at 3.64 eV(monitored at 420 nm) and $Ce2^{3+}$ center excited at 3.26 eV(monitored at 480 nm).

The decay times of $Ce1^{3+}$ band and $Ce2^{3+}$ band are measured to be 24 ns and 5 ns, respectively, and these results are consistent with those of ref.[6]. A drastic change in the decay curves was observed for the excitation photon energies in the range of $Eg < h\nu < 30$ eV; i.e. the decay curves including the initial build-up and the decay strongly depend on $h\nu$. The apparent decay time is 58 ns for an excitation just above the band gap energy of 6.2 eV and increases to the maximum value of 92 ns at $h\nu = 7.0$ eV and then decreases to 60 ns at $h\nu = 10.0$ eV. For 10.0 eV< $h\nu$ < 30.0 eV, it tends to 60 ns. The maximum rise time is observed at $h\nu = 7.0$ eV. The initial build-up time t_b that from 10% to 90 % of the peak intensity and the apparent decay time t_a are shown in Fig.2.

Those results are interpreted in terms of the excitation from the ground $^8S_{7/2}$ state of Gd^{3+} ion into the higher excited multiplets of 6.27 eV to 7.41 eV and form the valence band into the conduction band [7].

Acknowledgements

The authors would like to express their gratitude to Dr. K.Fukui of UVSOR facility for his assistance to perform the experiment at UVSOR.

References

[1] A. Lempicki, A.J. Wojtowicz and E. Berman, Nucl. Instr. and Meth. A 333 (1993) 304.

[2] T. Doke, E. Shibamura and S. Kubota, J. Phys. Soc. Jap. 68 (1999) 2433.

[3] H. Ishibashi, Nucl. Intstr. and Meth. A294 (1990)271.

[4] Z.A. Racholo, I.A. Tale, V.D. Ryzhikov, J.L. Jansons and S.F. Burochas, Nucl. Trans Radiat. Meas. 21 (1993) 121.

[5] H. Suzuki, T.A. Tombrello, C.L. Melcher and J.S. Schweitzer, Nucl. Instr. and Meth. A 320 (1992)263.

[6] H. Suzuki, T.A. Tombrello, C.L. Melcher, C.A. Peterson and J.S. Schweitzer, Nucl. Instr. and Meth. A 346(1994)510.

[7] S.Shimizu, H.Ishibashi, A. Ejiri and S. Kubota, Nucl. Instr. and Meth. (2002), in press.

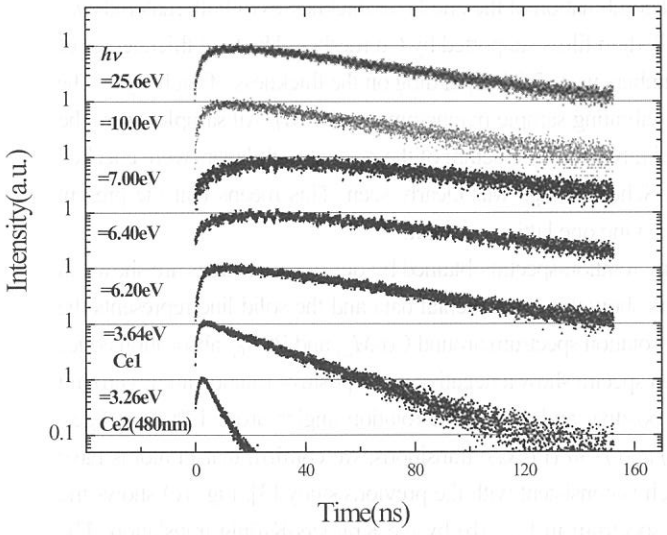

Fig.1. Decay curves of 0.5 mol % Ce-doped GSO under excitations by photons of various energies.

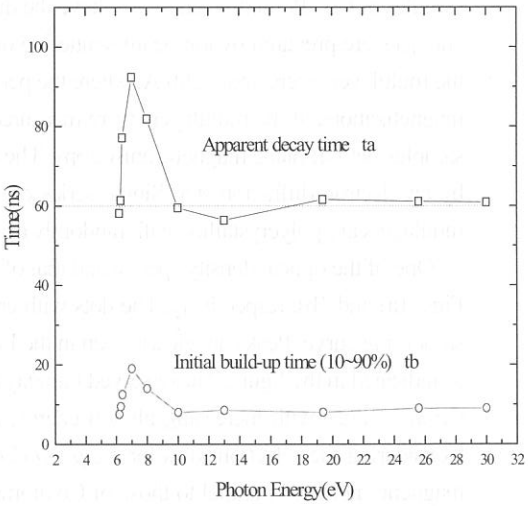

Fig.2. Apparent decay time and initial build-up times (10~90%) from 0.5 mol % Ce-doped GSO as a function of excitation photon energy. The curves are drawn only to guide the eyes. The dotted straight line is the expected decay time ~60 ns for sufficiently large photon energy.

(BL8B1)

Extreme Ultraviolet Faraday Rotation Spectra of Co / Pt Multilayers on Collodion Films

M. Igeta, K. Saito, T. Ejima, T. Hatano and M. Watanabe

Institute of Multidisciplinary Research for Advanced Materials, Tohoku University
Katahira 2-1-1, Aoba-ku, Sendai 980-8577, Japan

Many magnetic multilayers have been studied by the magnetic circular dichroism (MCD) measurements in the extreme ultraviolet, soft X-ray and hard X-ray regions. Among them, Co / Pt multilayers carefully grown to <111> direction have been investigated intensively to clarify the origin of their novel character of the perpendicular magnetic anisotropy (PMA) [1-3]. In the previous work by Nakajima *et al.* [3], it was proposed that the PMA is caused by the Co 3*d* - Pt 5*d* hybridization, which is highly localized at the Co / Pt interface. So it is interesting to investigate the magnetic properties and hybridization effect of Co / Pt multilayers grown to other directions without special treatment.

The Faraday rotation measurements on Co / Pt multilayers on collodion films were performed in the 55-80 eV region. The degree of linear polarization of the incident beam was more than 96 % in the energy region of the present experiment. The full bandwidth of the monochromatized incident beam was about 0.1 eV. The Faraday rotation apparatus consists of a magnetic circuit, a sample holder and a rotating analyzer unit [4]. A field of 8.2 kOe was generated by the magnetic circuit composed of four Sm / Co permanent magnets. The samples are situated, as the multilayer plane was perpendicular to the magnetic field. The polarization states of incident and transmitted beams were monitored by a rotating analyzer unit mounting Al / YB_6 and Mo / Si reflection multilayer polarizers. Twelve samples of Co / Pt multilayers which have the different combination of the one-layer thicknesses of both materials (t_{Co} and t_{Pt}) were prepared by ion-beam-sputtering onto collodion films supported by Cu meshes. The total thicknesses of the multilayers were about 200 Å, where the period numbers were 5-24 depending on the thickness of each layer. The magnetizations of the multilayers were measured by a vibrating sample magnetometer (VSM). All samples were the samples with in-plane magnetic anisotropy. The crystallinity and the structure of the present multilayers were checked by an electron diffractometer. Single series of Debye-Scherrer rings was clearly seen. This means that the present mutilayers are polycrystalline with randomly oriented having one lattice constant.

One of the optical density spectra and that of Faraday rotation spectra obtained by our measurements are shown in Figs. 1a) and 1b), respectively. The dots with error bars show the experimental data and the solid line represents the smoothing curve. Peaks are clearly seen in the Faraday rotation spectrum around Co-$M_{2,3}$ and Pt-$N_{6,7}$ absorption edges as indicated in the figure. The observed Faraday rotation spectra show a negative and a positive rotation angles around Co-$M_{2,3}$ edges with increasing photon energy, and a positive and a negative rotation angles around Pt-$N_{6,7}$ edges. Considering the selection rules for the $p \rightarrow d$ (Co-$M_{2,3}$) and $f \rightarrow d$ (Pt-$N_{6,7}$) transitions, we confirm that Pt atoms have magnetic moments parallel to those of Co atoms, which is consistent with the previous study [3]. Fig. 1c) shows the MCD spectrum calculated from the Faraday rotation spectrum in Fig. 1b) by the Kramers-Krönig translation. The spectral shape at the Pt-$N_{6,7}$ edges is somewhat different from that of the previous result [3], but similar to that of $CoPt_3$ alloy which shows the unusual profile due to the Fano effect [5]. Therefore, in the present experiment, the magnetization state in Pt seems to be similar to that in $CoPt_3$ alloy. However, the ratio of the MCD magnitudes for Co-$M_{2,3}$ and Pt-$N_{6,7}$ edges is about 1/3 in $CoPt_3$ alloy, but about 1 in the present multilayer, of which t_{Co} / t_{Pt} is about 1/3, so that the present samples are not $CoPt_3$ alloy.

Here, we assume that the peak-to-peak values of Faraday rotation angles around Co-$M_{2,3}$ and Pt-$N_{6,7}$ edges are proportional to the total magnetic moments of Co and Pt layers, respectively. In Figs. 2a) and 2b), the peak-to-peak values of the rotation angles around Co-$M_{2,3}$ edges per unit thickness of Co layer (normalized by the total thickness of the Co layers) and those around Pt-$N_{6,7}$ edges per unit thickness of Pt layer (normalized by the total thickness of the Pt layers) are plotted against the Co and Pt one-layer thicknesses (t_{Co} and t_{Pt}), respectively. Except for the samples with 3 Å thick Co one-layer, the peak-to-peak values for Co-$M_{2,3}$ edges per unit thickness of Co layer are almost the same,

but decrease gradually with the increase in Co one-layer thickness. The similar behavior was found in the case for Pt-$N_{6,7}$ edges. This means that each magnetic moment of Co and Pt atoms is almost constant, so that the magnetization of Co and Pt is not localized at the interface, but volumetric in our case. The reason why the values decrease with the increase in Co one-layer thickness may be due to the fact that the out-of-plane magnetization of these samples are not saturated, which was checked by the VSM. For the samples with 3 Å thick Co one-layer, rapid decrease with the increase in Pt one-layer thickness may be due to the disordered-alloying effect at the interface, where Co atoms become minor and are dispersed among Pt atoms.

In summary, the magnetization of Pt is not localized at the Co / Pt interface, but volumetric in the present samples. The state of hybridization is similar to that of $CoPt_3$. This conclusion is different from the previous experiment [3], which may be due to the difference in the growth direction and suggests that the PMA manifests itself in the multilayers grown to <111> direction.

References

[1] D. Weller, Y. Hu, J. Shöhr, M. G. Samant, B. D. Hermsmeier, C. Chappert, Phys. Rev. B **49** (1994) 12888.

[2] J. Thiele, C. Boeglin, K. Hricovini, F. Cheyrier, Phys. Rev. B **53** (1996) 11934.

[3] N. Nakajima, T. Koide, T. Shidara, H. Miyauchi, H. Fukutani, A. Fujimori, K. Ito, T. Katayama, M. Nývlt, Y. Suzuki, Phys. Rev. Lett. **81** (1998) 5229.

[4] T. Hatano, W. Hu, K. Saito, M. Watanabe, J. Electr. Spectr. Rel. Phenom. **101-103** (1999) 287.

[5] T. Shishidou, S. Imada, T. Muto, F. Oda, A. Kimura, S. Suga, T. Miyahara, T. Kanomata, T. Kaneko, Phys. Rev. B **55** (1997) 3749.

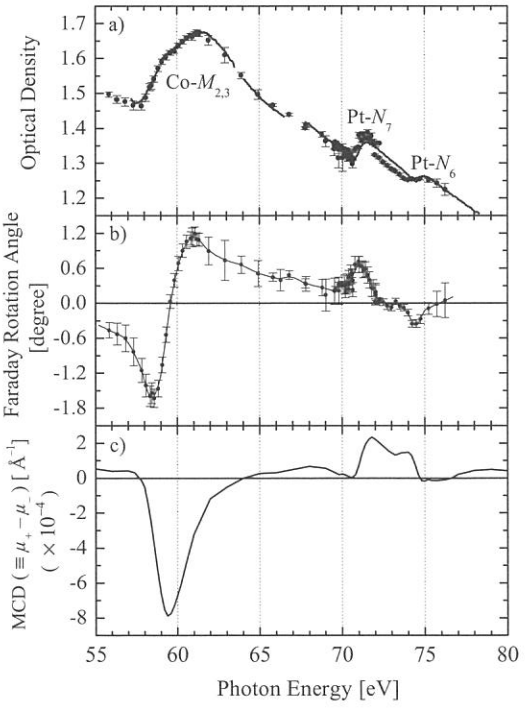

Fig. 1. a) Absorption and b) Faraday rotation spectra of Co (22.0 Å) / Pt (13.8 Å) multilayer in the 55-80 eV region, and c) MCD spectrum calculated from the Faraday rotation spectrum by the Kramers-Krönig translation.

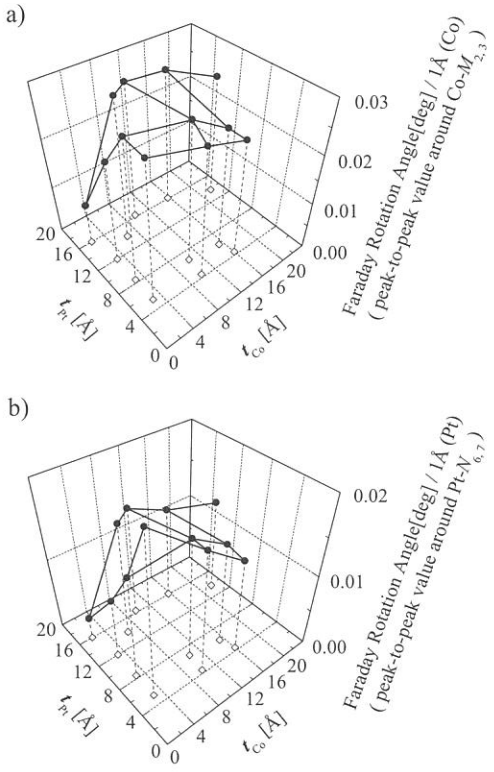

Fig. 2. a) Faraday rotation angles around Co-$M_{2,3}$ absorption edges per 1 Å thick Co layer and b) those around Pt-$N_{6,7}$ absorption edges per 1 Å thick Pt layer, as functions of Co and Pt one-layer thicknesses (t_{Co} and t_{Pt}).